The Astronomical Journal, 153:18 (15pp), 2017 January doi:10.3847/1538-3881/153/1/18

PLANETS AROUND LOW-MASS STARS (PALMS). VI. DISCOVERY OF A REMARKABLY RED PLANETARY-MASS COMPANION TO THE AB DOR MOVING GROUP CANDIDATE 2MASS J22362452+4751425*

Brendan P. Bowler[1,2,9], Michael C. Liu[3], Dimitri Mawet[2], Henry Ngo[2], Lison Malo[4], Gregory N. Mace[1], Jacob N. McLane[1], Jessica R. Lu[5], Isaiah I. Tristan[1,6], Sasha Hinkley[7], Lynne A. Hillenbrand[2], Evgenya L. Shkolnik[8], Björn Benneke[2], and William M. J. Best[3,10]

[1] McDonald Observatory and the Department of Astronomy, The University of Texas at Austin, Austin, TX 78712, USA; bpbowler@astro.as.utexas.edu
[2] California Institute of Technology, 1200 E. California Boulevard, Pasadena, CA 91125, USA
[3] Institute for Astronomy, University of Hawai'i at Mānoa; 2680 Woodlawn Drive, Honolulu, HI 96822, USA
[4] CNRS, CFHT, 65-1238 Mamalahoa Hwy Kamuela, HI 96743, USA
[5] Astronomy Department, University of California, Berkeley, CA 94720-3411, USA
[6] Department of Physics and Astronomy, Rice University, MS-108, 6100 Main Street, Houston, TX 77005, USA
[7] University of Exeter, Physics and Astronomy, EX4 4QL Exeter, UK
[8] School of Earth and Space Exploration, Arizona State University, Tempe, AZ 85287, USA
Received 2016 August 28; revised 2016 October 12; accepted 2016 October 31; published 2016 December 21

ABSTRACT

We report the discovery of an extremely red planetary-mass companion to 2MASS J22362452+4751425, a $\approx$0.6 $M_{\odot}$ late-K dwarf likely belonging to the $\sim$120 Myr AB Doradus moving group. 2M2236+4751 b was identified in multi-epoch NIRC2 adaptive optics imaging at Keck Observatory at a separation of 3.″7, or 230 $\pm$ 20 AU in projection at the kinematic distance of 63 $\pm$ 5 pc to its host star. Assuming membership in the AB Dor group, as suggested from its kinematics, the inferred mass of 2M2236+4751 b is 11–14 $M_{\rm Jup}$. Follow-up Keck/OSIRIS K-band spectroscopy of the companion reveals strong CO absorption similar to other faint red L dwarfs and lacks signs of methane absorption, despite having an effective temperature of $\approx$900–1200 K. With a $(J–K)_{\rm MKO}$ color of 2.69 $\pm$ 0.12 mag, the near-infrared slope of 2M2236+4751 b is redder than all of the HR 8799 planets and instead resembles the $\approx$23 Myr isolated planetary-mass object PSO J318.5–22, implying that similarly thick photospheric clouds can persist in the atmospheres of giant planets at ages beyond 100 Myr. In near-infrared color–magnitude diagrams, 2M2236+4751 b is located at the tip of the red L dwarf sequence and appears to define the "elbow" of the AB Dor substellar isochrone separating low-gravity L dwarfs from the cooler young T dwarf track. 2M2236+4751 b is the reddest substellar companion to a star and will be a valuable benchmark to study the shared atmospheric properties of young low-mass brown dwarfs and extrasolar giant planets.

Key words: planetary systems – planets and satellites: atmospheres – stars: individual (2MASS J22362452+4751425) – stars: low-mass

1. INTRODUCTION

L dwarfs with anomalously red near-infrared colors were first identified in the Two Micron All-Sky Survey (2MASS; Skrutskie et al. 2006) over a decade ago (Dahn et al. 2002) and have steadily grown as a population ever since. With some notable exceptions (e.g., Looper et al. 2008; Marocco et al. 2014), these objects were generally found to possess low-surface gravity features in their optical and near-infrared spectra, pointing to ages much younger than the the vast majority of brown dwarfs in the field (McLean et al. 2003; Kirkpatrick et al. 2006; Kirkpatrick et al. 2008). In recent years, the sample of red L dwarfs has ballooned (Reid et al. 2008; Geißler et al. 2011; Gizis et al. 2012; Liu et al. 2013b; Mace et al. 2013; Thompson et al. 2013; Marocco et al. 2014; Schneider et al. 2014; Best et al. 2015; Kellogg et al. 2016; Schneider et al. 2016) as a result of all-sky infrared surveys like the *Wide-field Infrared Survey Explorer* (*WISE*), Panoramic Survey Telescope and Rapid Response System (Pan-STARRS), UKIRT Infrared Deep Sky Survey, and Visible and Infrared Survey Telescope for Astronomy (VISTA), inspiring new gravity-insensitive spectral classification systems, all-sky searches for young brown dwarfs, and infrared parallax programs to better determine their physical properties and relationship with young moving groups (Cruz et al. 2009; Allers & Liu 2013; Liu et al. 2013a; Gagné et al. 2014; Gagné et al. 2015b; Aller et al. 2016; Faherty et al. 2016).

It is now clear that these low-gravity brown dwarfs lie on a parallel sequence redward of the standard L dwarf locus in near-infrared color–magnitude diagrams. Liu et al. (2016, in press) show that the ensemble of late-M and L dwarfs with very low-gravity spectral classifications represent a "fanning out" of old field objects with the same spectral type; later-type young L dwarfs are progressively redder and fainter in M_J than their higher-gravity counterparts. This systematic offset and broadening of the L dwarf locus is likely caused by a combination of youthful overluminosity for late-M and early-L dwarfs and unusually dusty photospheres at later types, which redistribute emergent flux to longer wavelengths (e.g., Filippazzo et al. 2015). While this narrative may be qualitatively correct, no set of self-consistent atmospheric and evolutionary models can completely reproduce the colors and spectra of this fascinating population.

* Some of the data presented herein were obtained at the W.M. Keck Observatory, which is operated as a scientific partnership among the California Institute of Technology, the University of California and the National Aeronautics and Space Administration. The Observatory was made possible by the generous financial support of the W.M. Keck Foundation.
[9] Hubble Fellow.
[10] Visiting Astronomer at the Infrared Telescope Facility, which is operated by the University of Hawaii under Contract NNH14CK55B with the National Aeronautics and Space Administration.

In parallel with discoveries of young isolated brown dwarfs, adaptive optics imaging surveys have identified a similar pattern of redder colors and fainter absolute magnitudes among young extrasolar giant planets (see, e.g., Bowler 2016). The archetypal companion in this class is 2M1207–3932 b (Chauvin et al. 2004); with a J–K color of 3.1 ± 0.2 mag (Dupuy & Liu 2012), it is the reddest ultracool object known and lacks the deep methane absorption expected at the effective temperature predicted by cooling models (Mohanty et al. 2007; Patience et al. 2010). More generally, this empirically discovered trait—not predicted beforehand by atmospheric models—is also seen in other red, low-temperature companions like HR 8799 bcde (e.g., Marois et al. 2008a; Bowler et al. 2010; Barman et al. 2011a; Skemer et al. 2014; Bonnefoy et al. 2016), 2M0122–2439 B (Bowler et al. 2013; Hinkley et al. 2015), and VHS J1256–1257 b (Gauza et al. 2015), as well as young free-floating brown dwarfs near the canonical L/T transition (e.g., Liu et al. 2013b) and may be caused by vigorous vertical mixing and strong disequilibrium carbon chemistry (Barman et al. 2011b; Zahnle & Marley 2014).

A natural question that has emerged from these studies is the degree to which young isolated brown dwarfs and extrasolar giant planets share common atmospheric properties and cooling pathways. The physical properties of the lowest-mass brown dwarfs appear to broadly overlap with the most massive giant planets. However, if the initial conditions or compositions of these populations are substantially different from one another as a result of disparate formation channels, then this similarity may be superficial and free-floating young red L dwarfs may not be "exoplanet analogs" after all. Unfortunately, the dearth of known red L dwarf companions currently prevents this kind of comparison.

Here, we present the discovery of an extraordinarily red companion to the late-K dwarf 2MASS J22362452+4751425. The host star was identified by Schlieder et al. (2012) as a candidate member of the AB Dor moving group on the basis of its proper motion and UV emission from *Galaxy Evolution Explorer* (*GALEX*). Our new radial velocity measurements of the primary are consistent with AB Dor membership, implying a mass of $\sim$11–14 $M_{\rm Jup}$ for the companion. At a separation of 3.″7 (230 AU), 2MASS J22362452+4751425 b (hereinafter 2M2236+4751 b) belongs to two classes of rare and enigmatic objects: planetary-mass companions on extremely wide orbits (>100 AU), which have low occurrence rates of <2% around young stars (Bowler 2016), and red L dwarf companions, of which only a handful are known. 2M2236+4751 b is likely to be an important benchmark for both populations.

2. OBSERVATIONS

2.1. Keck/NIRC2 Adaptive Optics Imaging

We first imaged 2M2236+4751 on 2014 November 8 UT in K_S-band with Keck/NIRC2 using natural guide star adaptive optics (NGS AO; Wizinowich 2013) as part of our ongoing efforts to find, characterize, and measure the statistical properties of giant planets around young low-mass stars. 2M2236+4751 b was identified at a separation of 3.″7 (Figure 1) and subsequently confirmed to be comoving with its host star through followup imaging in 2015 and 2016 (Table 1). All observations were carried out in a similar manner with the narrow camera using the entire 1024×1024 pix^2 array, the partly translucent 600 mas diameter coronagraph,

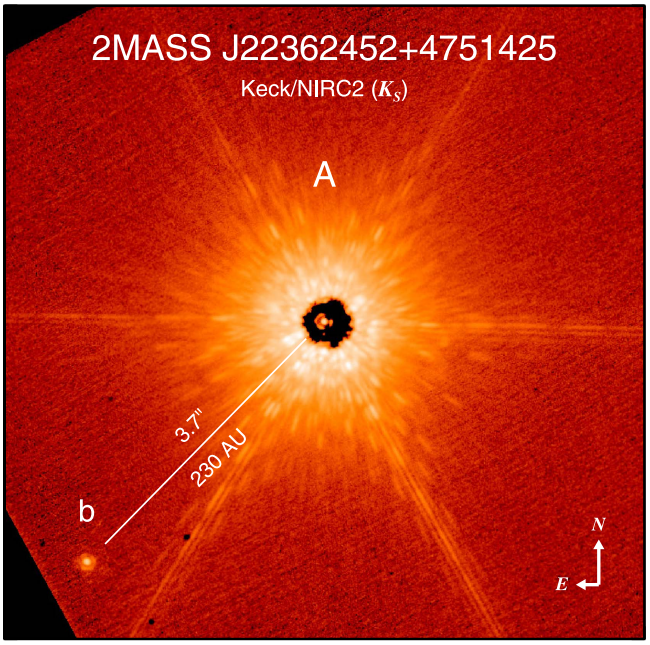

Figure 1. Single NIRC2 K_S-band image of 2M2236+4751 Ab from 2015 August. The K7 host star is positioned behind the partly translucent 600 mas diameter coronagraph. 2M2236+4751 b is located at a separation of 3.″7 near the edge of the array in this $7'' \times 7''$ image. North is up and east is to the left.

and the vertical angle (pupil-tracking) rotator setup. In addition to coronagraphic imaging, we also acquired 10–20 unsaturated frames of the host star for photometric calibration immediately before or after the deeper imaging, except on 2016 June 27 UT (K_S filter) and 2016 July 18 UT (H filter); for these data sets we use the coronagraph transmission measurement from Bowler et al. (2015) to derive the flux ratios of 2M2236+4751 Ab.

Raw images were bias-subtracted, flat-fielded, and corrected for bad pixels and cosmic rays. Field rotation was small (between 2° and 6°) in our 5–10 minute sequences and the companion is outside of the speckle noise-limited region close to the star, so no angular differential imaging subtraction was necessary. Each frame was corrected for optical distortions using the solution from Yelda et al. (2010) for data obtained prior to 2015 April and from Service et al. (2016) thereafter to account for the altered optical distortion following a NIRC2 pupil realignment. The corresponding plate scales and north orientation angles are 9.952 ± 0.002 mas pix^{-1} and $+0.^{\circ}252 \pm 0.^{\circ}009$ from Yelda et al., and 9.971 ± 0.004 mas pix^{-1} and $+0.^{\circ}262 \pm 0.^{\circ}02$ from Service et al. The images were registered using the position of the host star visible behind the occulting mask and were then derotated, median-combined, and north-aligned to produce a final reduced frame (Figure 2).

Astrometry of the companion is derived in a similar manner as in Bowler et al. (2015) and takes into account positional uncertainties of the star behind the coronagraph, centroid errors of the companion, and systematic errors in the distortion solution and north alignment, the latter of which is the dominant term in the error budget. When unsaturated frames were obtained, relative photometry was measured by calculating the mean and standard deviation of counts from the host star in the unsaturated images and from the companion in the deep coronagraphic data using aperture photometry. Photometric uncertainties are propagated analytically. Our NIRC2 astrometry and relative photometry are listed in Table 1.

Table 1
Keck/NIRC2 Adaptive Optics Imaging of 2MASS J22362452+4751425

UT Date	Epoch (UT)	$N \times$ Coadds $\times$ t_{exp} (s)	Filt.	Sep. (mas)	P.A. (°)	Δmag	FWHM[a] (mas)
2014 Nov 08	2014.852	5 × 1 × 60	K_S+cor600	3692 ± 3	135.8 ± 0.2	7.3 ± 0.5	69 ± 9
2015 Aug 27	2015.653	5 × 1 × 60	K_S+cor600	3694 ± 3	135.7 ± 0.2	8.22 ± 0.04	48 ± 1
2016 Jun 27	2016.489	10 × 1 × 60	K_S+cor600	3696 ± 3	135.3 ± 0.2	8.2 ± 0.3	⋯
2016 Jun 27	2016.489	10 × 1 × 60	H+cor600	3705 ± 3	134.8 ± 0.2	9.8 ± 0.4	41 ± 1
2016 Jul 18	2016.546	10 × 10 × 6	H+cor600	3707 ± 3	135.4 ± 0.2	9.0 ± 0.2	⋯
2016 Jul 19	2016.549	10 × 6 × 10	J+cor600	3705 ± 3	135.7 ± 0.2	10.4 ± 0.3	34 ± 1
2016 Aug 03	2016.590	2 × 1 × 60	J+cor600	3690 ± 3	135.4 ± 0.2	9.93 ± 0.12	36 ± 1

Note.
[a] FWHM of 2M2236+4751 A as measured from unsaturated frames.

Table 2
Spectroscopic Observations

Object	Date (UT)	Telescope/ Instrument	Filter	Slit Width (″)	Plate Scale (mas pix^{-1})	Tot. Exp. (minutes)	Resolution (=λ/Δλ)	Standard[a]
2M2236+4751 A	2016 Jun 13	CFHT/ESPaDOnS	⋯	⋯	⋯	15	68000	⋯
2M2236+4751 A	2016 Jun 14	McDonald 2.7 m/IGRINS	⋯	0.98	⋯	32	45000	HD 219290
2M2236+4751 A	2016 May 24	IRTF/SpeX (SXD)	⋯	0.3	⋯	4	2000	HD 209932
2M2236+4751 b	2016 Jun 23	Keck/OSIRIS	*Kbb*	⋯	50	60	3800	HD 172728

Note.
[a] Radial velocity standard or telluric standard.

2.2. Keck/OH-Suppressing Infrared Imaging Spectrograph (OSIRIS) Spectroscopy of 2M2236+4751 b

We obtained a medium-resolution ($R \equiv \lambda/\Delta\lambda \approx 3800$) 1.96–2.38 μm spectrum of 2M2236+4751 b with OSIRIS (Larkin et al. 2006) mounted on Keck I and coupled with NGS AO on 2016 June 23 UT (Table 2). Our observations benefited from a new grating installed in 2012 (Mieda et al. 2014) and a new spectrograph detector in early 2016, a few months prior to our observing run. Observations were taken with the *Kbb* filter and the 50 mas pix^{-1} plate scale, resulting in a 16 × 64 spaxel^2 (spatial pixel) lenslet geometry and 0.″8 × 3.″2 rectangular field of view. The rotator was set orthogonal to the binary position angle (P.A.) to avoid contamination from the host star. We acquired six pairs of nodded data cubes in an AB pattern with individual exposures of 300 s, totaling 60 minutes of on source integration time altogether. Conditions were clear with 0.″4 seeing throughout our science observations. Immediately prior to this, we observed the A0V standard HD 172728 for telluric correction.

The raw 2D images were transformed to 3D data cubes with the OSIRIS data reduction pipeline and the latest rectification matrices from Keck. Spectra were extracted using aperture photometry with local sky subtraction then scaled to a common level and median-combined. Telluric correction was carried out with the `xtellcor_general` routine in the Spextool reduction package for IRTF/SpeX (Vacca et al. 2003; Cushing et al. 2004). Finally, our spectrum was flux calibrated using a multiplicative scale factor corresponding to the apparent K_S magnitude measured with NIRC2.

2.3. CFHT/ESPaDOnS Optical Spectroscopy

High-resolution optical spectroscopy was obtained for 2M2236+4751 A in queue service observing (QSO) mode with ESPaDOnS (Donati et al. 2006) at CFHT on 2016 June 13 UT. ESPaDOnS was used in the Star+Sky spectroscopic mode and combined with the normal CCD readout mode to yield a resolving power of $R \sim 68{,}000$ covering the 3700–10500 Å wavelength range. The total integration time was 900 seconds. The data were reduced by the QSO team using the CFHT pipeline UPENA1.0, which uses the Libre-ESpRIT software package (Donati et al. 1997). A heliocentric radial velocity of –22.1 ± 0.5 km s^{-1} and a projected rotational velocity of 4 km s^{-1} were measured using the same methodology as described in Malo et al. (2014).

2.4. Harlan J. Smith Telescope/IGRINS Spectroscopy

We observed 2M2236+4751 A with the Immersion Grating Infrared Spectrometer (IGRINS) on the 2.7 m Harlan J. Smith telescope located at McDonald Observatory. IGRINS is a high-resolution near-infrared spectrograph offering simultaneous coverage of the H and K bands (1.45–2.45 μm) at a resolution of $R \simeq 45{,}000$ (Park et al. 2014). Observations consisted of four 480 s exposures taken in an ABBA nod pattern. Immediately after, we observed the A0V star HD 219290 at a similar airmass for telluric correction.

The IGRINS data were reduced using version 2.1 of the IGRINS reduction pipeline[11] (Lee & Gullikson 2016). The pipeline performs dark, bias, and flat corrections, followed by an optimal extraction of the 1D spectrum for both the target and A0V star. A first-order wavelength solution is generated using lines from a ThAr lamp; a full wavelength solution is then generated using OH emission sky lines. Finally, a more refined wavelength solution is calculated using telluric absorption lines in the raw A0 spectrum. The final spectrum has an S/N of ∼150 per resolution element.

[11] https://github.com/igrins/plp

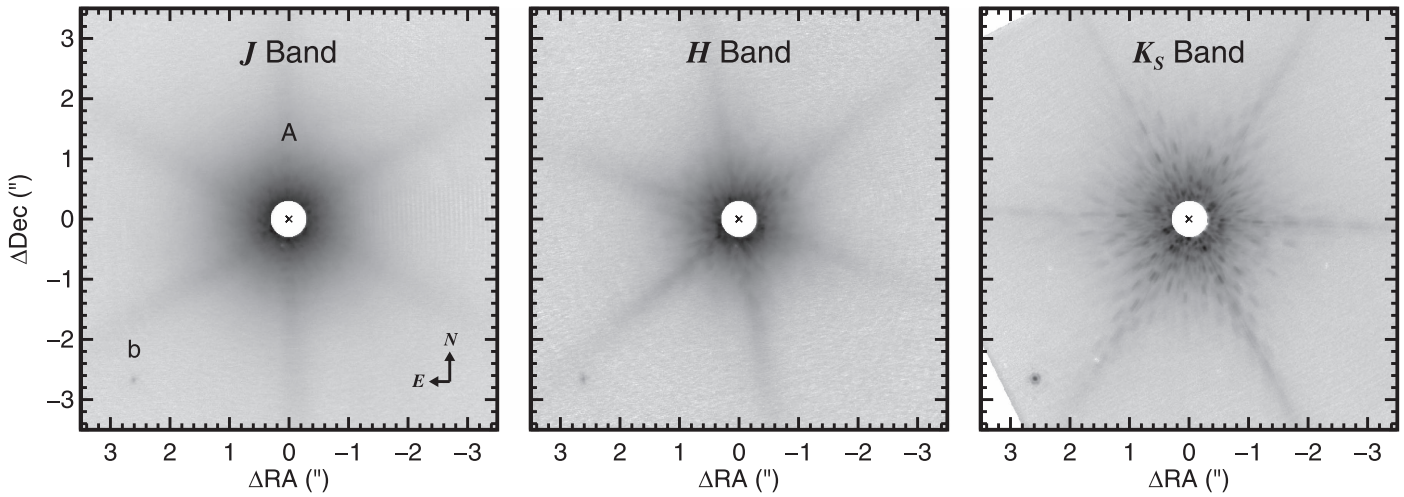

Figure 2. Median-combined NIRC2 images of 2M2236+4751 Ab in *J*, *H*, and K_S filters from 2016 July, 2016 June, and 2015 August, respectively. 2M2236+4751 b is unusually red with a J–K_S color of 2.7 mag. Individual frames were derotated before being combined and north-aligned to correct for a small amount of rotation experienced in pupil-tracking mode. This resulted in a slight azimuthal blurring of the host star, which is especially evident in *J* and *H* bands. The position of the host star is marked with an "x." Images have been stretched with an inverse hyperbolic sine transformation. North is up and east is to the left.

The broad spectral grasp of IGRINS provides more than 20,000 resolution elements at $R \simeq 45{,}000$. Cross-correlation of all of these elements provides robust statistical measurements of stellar radial velocities. As described in Mace et al. (2016), the spectral stability of IGRINS is subpixel within an observing night, producing a radial velocity precision of $<200\,\mathrm{m\,s^{-1}}$. Radial velocities have been derived for nearly all IGRINS observations. Briefly, the IGRINS spectrum of 2M2236+4751 A was cross-correlated in pixel space against 144 other IGRINS spectra with spectral types between K3 and M2. Shifts in the spectrum are removed by cross-correlating the telluric spectra to determine pixel shifts between the target and the templates with similar spectral type. Pixel offsets between stellar spectra are converted into velocities using the empirically derived spectral resolution. The relative radial velocity is determined from the mean and standard error of all radial velocity measurements from all 144 template spectra, after a sigma filter, which removes $>4\sigma$ outliers. The relative radial velocity is converted into an absolute radial velocity using a zero-point shift based on >100 absolute radial velocities from the literature. Our final barycentric radial velocity for 2M2236+4751 A is $-21.4 \pm 0.2\,\mathrm{km\,s^{-1}}$, consistent with (and more precise than) the CFHT/ESPaDOnS measurement.

2.5. IRTF/SpeX Near-infrared Spectroscopy

To better characterize the host star, we obtained a medium-resolution 0.7–2.55 μm spectrum of 2M2236+4751 A on 2016 May 24 UT with the short cross-dispersed mode of the recently upgraded SpeX (Rayner et al. 2003) spectrograph at the NASA Infrared Telescope Facility (IRTF). The 0.″3 slit was used, which resulted in an average resolving power of $R \approx 2000$. Four pairs of 30 s exposures were taken in an ABBA pattern along the 15″ slit. The A0V standard HD 209932 was observed immediately beforehand at a similar airmass. Images were pairwise subtracted and then the spectra were extracted, median-combined, and corrected for telluric features using the Spextool reduction package (Vacca et al. 2003; Cushing et al. 2004).

3. RESULTS

3.1. Common Proper Motion

Our NIRC2 astrometry of 2M2236+4751 Ab spans 1.7 years (Table 1). Throughout this period, the expected change in separation and P.A. for a stationary background star are 119 ± 5 mas and $1\overset{\circ}{.}0 \pm 0\overset{\circ}{.}3$, respectively, based on our first epoch of astrometry, the host star's proper motion from UCAC4 ($\mu_\alpha \cos\delta = 62.6 \pm 1.4\,\mathrm{mas\,yr^{-1}}$, $\mu_\delta = -30.5 \pm 1.9\,\mathrm{mas\,yr^{-1}}$; Zacharias et al. 2013), and its kinematic distance (63 ± 5 pc; Section 3.2). The measured change between the initial and latest epochs is only 2 ± 4 mas and $0\overset{\circ}{.}4 \pm 0\overset{\circ}{.}3$, heavily favoring the common proper motion scenario (Figure 3).

The comoving versus stationary background hypotheses can be tested more quantitatively using the Bayes factor. Following Bowler et al. (2013), the χ^2 values of the comoving (M_1) and stationary (M_2) scenarios are 30 and 2850, respectively, for five degrees of freedom. Assuming equivalent prior odds, the posterior odds are $\log(P(M_1)/P(M_2)) = 613$, indicating the pair are unambiguously comoving and very likely to be gravitationally bound.

3.2. Age and Young Moving Group Membership

The age of 2M2236+4751 is critical to the interpretation of this system; a young age would imply that the companion has a mass in the planetary regime and its red colors are the result of thick clouds associated with low surface gravity like 2M1207–3932 b, while an old age would indicate that it is a brown dwarf with an unusually dusty (and potentially metal-rich) photosphere like 2M2148+4003 (Looper et al. 2008). Here, we discuss two lines of evidence regarding the system age: a potential kinematic link to the ≈120 Myr AB Dor moving group, and other age indicators like activity and rotation period.

Schlieder et al. (2012) identified 2M2236+4751 as a candidate member of the AB Dor moving group from its proper motion and sky position. We also find consistency with AB Dor using an alternative method to identify new members of young moving groups (B. Bowler et al. 2017, in preparation). By adopting the *UVW* kinematics and uncertainties of moving

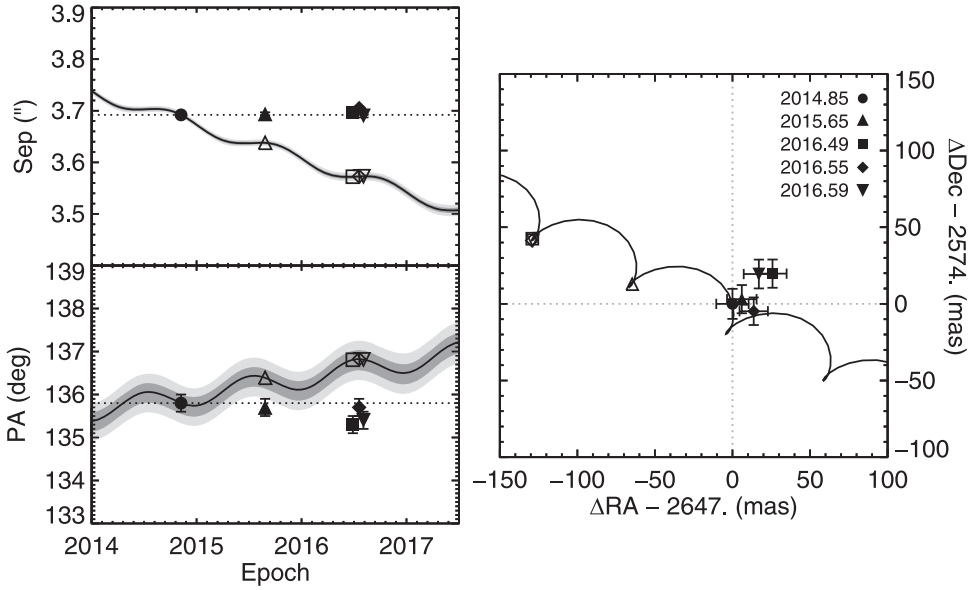

Figure 3. Expected relative motion of a stationary background object (solid curve) based on the proper and parallactic motion of 2M2236+4751 A. Our measured astrometry (filled symbols) is consistent with a constant separation and P.A. (dotted lines) for 2M2236+4751 b over time, indicating it is comoving with its host star. Open symbols show the expected positions of 2M2236+4751 b if it were stationary for each epoch of our observations. Gray shaded regions denote 1-σ and 2-σ confidence intervals for the background tracks, which incorporate uncertainties in our first epoch astrometry, kinematic distance, and host star proper motion.

groups from Torres et al. (2008), we can invert the standard calculation of galactic space velocities (Johnson & Soderblom 1987) when only a proper motion is available to predict an expected radial velocity distribution as well as two distance distributions associated with each proper motion component ($\mu_\alpha \cos\delta$ and μ_δ). These two distance distributions should agree with one another if the object is a member of a particular group being tested; subtracting one from the other and calculating the tail integral about zero offers a simple metric ($\mathcal{M}$) to assess this consistency. $\mathcal{M}$ values near 0.5 are most consistent, while incompatible distributions have $\mathcal{M}$ values near 0.

For 2M2236+4751 we find an $\mathcal{M}$ value of 0.45 for AB Dor and values of 0.0 for the TWA, β Pic, Tuc-Hor, Columba, and Carina moving groups, indicating excellent proper motion consistency with the AB Dor moving group (Figure 4). To assess the false positive probability that non-moving group members would have $\mathcal{M}$ values at least this high by chance, we ran the same analysis for a sample of over 2000 inactive M dwarfs from Gaidos et al. (2014). The probability that a field star would share a similarly consistent proper motion with the AB Dor moving group is 1.1%. We adopt this as an upper limit, because the joint probability of a similar proper motion *and* radial velocity (see below) will be substantially smaller than this. Note that one difference between our method and Bayesian techniques is that our approach does not rely on probabilistic assignments using kinematic (*UVW*) and positional (*XYZ*) models for moving groups and field stars. For example, the BANYAN I algorithm developed by Malo et al. (2013) predicts a probability of 68% for AB Dor membership, but BANYAN II (which uses updated membership lists and is tailored to low-mass moving group members; Gagné et al. 2014) gives an AB Dor probability of only 0.11%.[12]

[12] The BANYAN I and II AB Dor membership probabilities increase to 84% and 0.9%, respectively, when also using the weighted mean radial velocity. The low probability from BANYAN II is likely based on the *Y* position of 2M2236 +4751 compared to bona fide AB Dor members, which we discuss in more detail later in this section. For reference, note that the BANYAN II "young field" and "old field" probabilities are 52% and 47%, respectively.

We find predicted (kinematic-based) radial velocity and distances of -22.8 ± 1.2 km s^{-1} and 63 ± 5 pc. This is in good agreement with our measured radial velocities from ESPaDOnS (-22.1 ± 0.5 km s^{-1}) and IGRINS (-21.4 ± 0.2 km s^{-1}), bolstering a possible kinematic association with AB Dor. Similarly, the photometric distance to 2M2236 +4751 is 74 ± 10 pc based on the M_V versus V–K_S relationship for the Pleiades from Bowler et al. (2013), which is $\approx 1\sigma$ from the kinematic distance. Our results are also consistent with the radial velocity and distance predictions of -23.0 ± 1.2 km s^{-1} and 65 ± 9 pc inferred by Schlieder et al.

Figure 5 shows the *UVW* galactic space velocities and *XYZ* heliocentric positions for 2M2236+4751 based on its proper motion, weighted mean radial velocity (-21.5 ± 0.2 km s^{-1}), and kinematic distance compared to confirmed members of nearby young moving groups from Gagné et al. (2014). The agreement with known AB Dor members in *U*, *V*, *W*, *X*, and *Z* is excellent, but the *Y* position appears to be an outlier. It is unclear how problematic this is, since the current census of moving group members is incomplete and heavily biased toward nearby ($\lesssim$60 pc) young stars owing to distance cuts in early searches (see, e.g., Zuckerman & Song 2004). Soon *Gaia* will reveal the entire stellar population and *UVW*/*XYZ* distributions of these nearby moving groups. Until then, we simply note this possible tension with the *Y* positional distribution of AB Dor members and await a re-evaluation in the future.

Activity diagnostics offer additional independent ways to constrain the age of this system. 2M2236+4751 was not detected in the *ROSAT* All-Sky Survey (RASS). Adopting an upper limit equal to the detection limit of RASS (0.05 cnts s^{-1}; Voges et al. 1999) and assuming a Hardness Ratio 1 (HR1) value of 0.0, the implied X-ray flux from 2M2236+4751 is $f_X < 4.1 \times 10^{-13}$ erg cm^{-2} s^{-1}, the X-ray luminosity is $\log(L_X) < 29.3$ erg s^{-1}, and the fractional X-ray to bolometric luminosity is $\log(L_X/L_{\rm bol}) <$

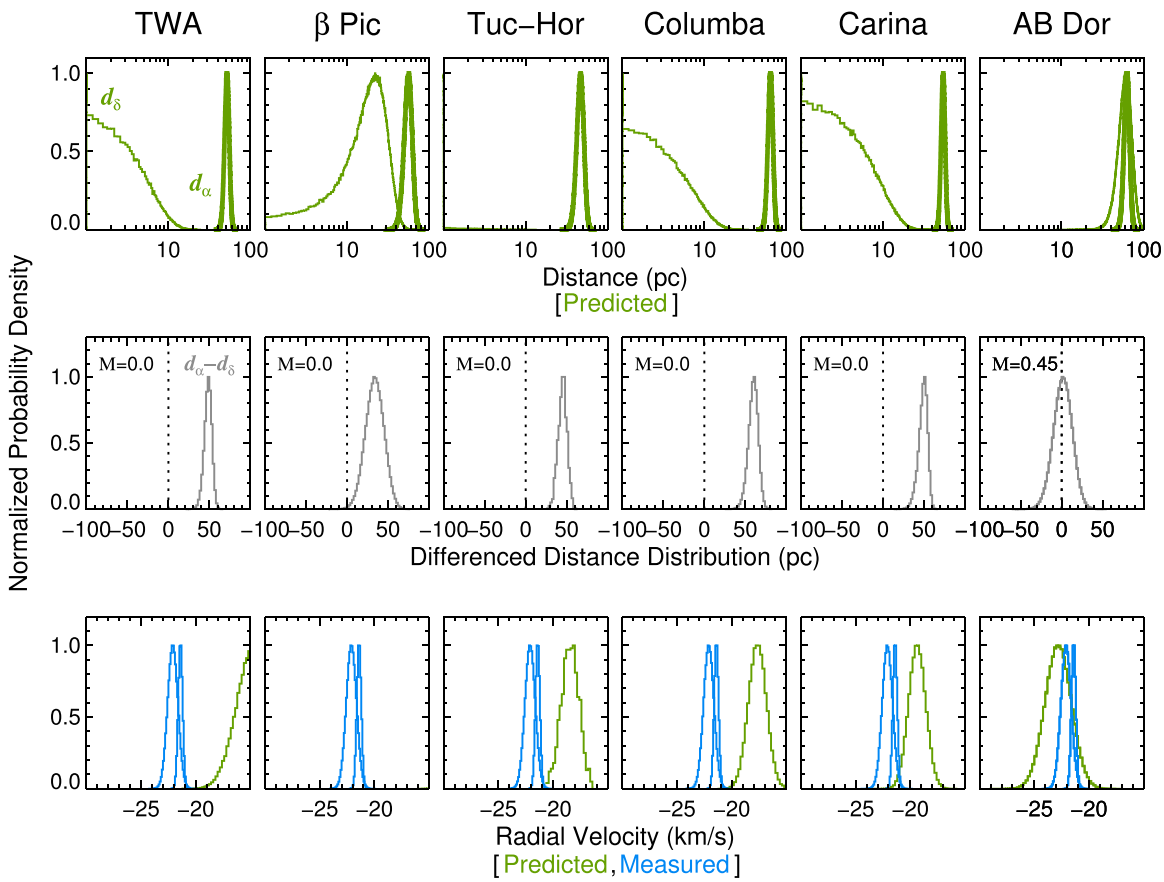

Figure 4. Young moving group membership tests based on the proper motion of 2M2236+4751. By adopting moving group *UVW* space velocities from Torres et al. (2008), the measured proper motion and sky position of 2M2236+4751 can be inverted to solve for the expected distance (for both R.A. and decl. proper motion components; top row) and the expected radial velocity (bottom row) assuming group membership. The middle row shows the difference of the two distance distributions; the agreement of the two is represented by the metric $\mathcal{M}$, which is the lower tail integral of the difference distribution about zero (B. Bowler et al. 2017, in preparation). 2M2236+4751 agrees well with AB Dor, but is inconsistent with all other moving groups tested here. Moreover, the measured radial velocity from ESPaDOnS and IGRINS (blue, bottom row) is consistent with the predicted value.

–3.1 dex.[13] These values are near the saturation limit for X-ray emission in low-mass stars, and so a non-detection in RASS is not particularly useful to constrain the coronal emission and age of 2M2236+4751. Low-mass Pleiades members span a wide range of X-ray luminosities, $\log(L_X/L_{\rm bol}) \approx -3$ to –4 dex (Preibisch & Feigelson 2005), and so this X-ray upper limit is consistent with a Pleiades (and AB-Dor)-like age of ∼120 Myr. Table 3 lists the activity levels for known or suspected K7 members of AB Dor; like Pleiades members, these objects have fractional X-ray luminosities between –3.0 and –4.0 dex, consistent with our upper limit for 2M2236+4751.

UV photometry from *GALEX* (Martin et al. 2005; Morrissey et al. 2007) provides another age diagnostic for 2M2236+4751. The host star is detected in the near-UV filter (NUV = 20.9 ± 0.2 mag), but not in the far-UV (FUV). Findeisen et al. (2011) show that older stars trace an envelope in NUV–*J* color as a function of near-infrared color; the NUV–*J* color of 10.9 ± 0.2 mag for 2M2236+4751 is generally consistent with Hyades-like chromospheric emission, but slightly redder than known K7 members in AB Dor with *GALEX* detections (Table 3). Similarly, the $F_{\rm FUV}/F_J$ ratio ($9 \pm 2 \times 10^{-5}$) from Shkolnik et al. (2011) and $(F_{\rm FUV}/F_J)_{\rm exc}$ excess ratio above the photosphere ($8 \pm 2 \times 10^{-5}$) from Shkolnik & Barman (2014) indicate that 2M2236+4751 has lower chromospheric emission levels than most stars at AB Dor-like ages. However, the large intrinsic scatter makes it difficult to rule out all but the youngest ages ($\lesssim$10 Myr) for this object.

The Hα equivalent width measured from our high-resolution ESPaDOnS spectrum is +0.18 ± 0.02 Å in absorption (Figure 6). A lack of Hα emission is consistent with 2M2236+4751's apparently weak chromospheric and coronal emission. This value is also somewhat weaker than the envelope traced out by older main sequence stars (≈–0.6 Å for a *B*–*V* color of 1.2 mag; see, e.g., Figure 5 of Zuckerman & Song 2004), indicating the Hα line may be slightly filled in for this star. Hα emission for K7 AB Dor members ranges from +0.3 to –1.3 Å (Table 3). A weak absorption line at about 6707.8 Å may be caused by either the Li I doublet or possibly Fe I at 6707.4 Å. If it originates from lithium, its equivalent width (EW = 40 ± 10 mÅ) is comparable to other AB Dor members with similar optical colors (e.g., Torres et al. 2008).

Stars spin up as they contract to the zero-age main sequence and then slowly spin down over time through magnetic braking and winds, and so in principle rotation periods offer another tool to constrain stellar ages. In practice, age determinations using rotation periods are imprecise for low-mass stars, because

[13] If, instead, we adopt an HR1 value of –0.3, which is the typical value for older field stars (Bowler et al. 2012), the resulting upper limits are $f_X < 3.4 \times 10^{-13}$ erg cm^{-2} s^{-1}, $\log(L_X) < 29.2$ erg s^{-1}, and $\log(L_X/L_{\rm bol}) < -3.2$ dex.

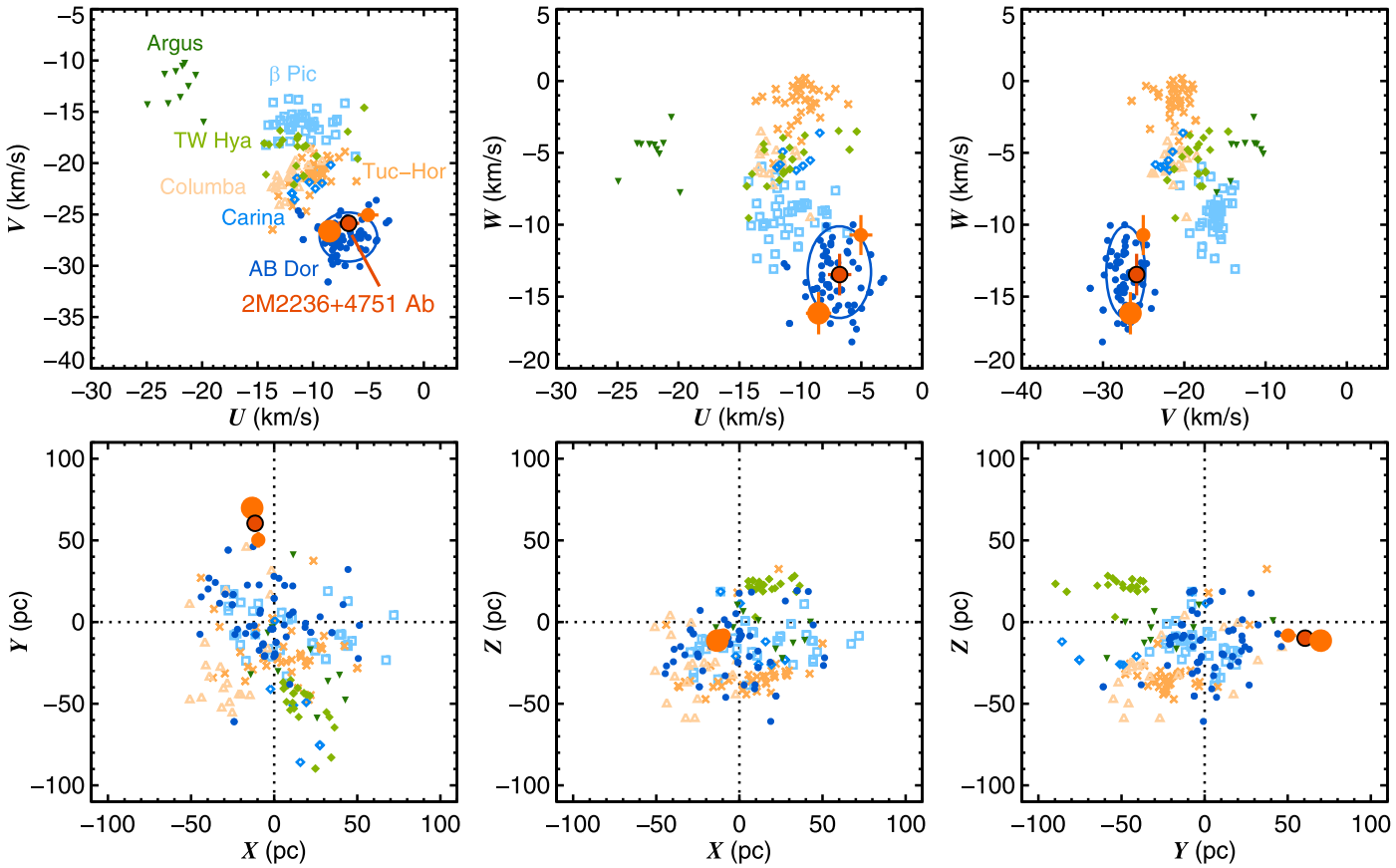

Figure 5. Partially constrained *UVW* galactic space velocities (top) and *XYZ* heliocentric positions (bottom) for 2M2236+4751 Ab compared to nearby young moving groups. Red circles denote distances of 53 ± 5 pc, 63 ± 5, and 73 ± 5 pc to 2M2236+4751 A based on its proper motion and weighted mean radial velocity. The space velocities of 2M2236+4751 Ab are in good agreement with known AB Dor members from Gagné et al. (2014) and the AB Dor locus from Torres et al. (2008, 2-σ ellipses). 2M2236+4751 Ab is similar to known members in *X* and *Z*, and lies just beyond the established population in the *Y* direction.

Table 3
K7 Dwarfs in the AB Dor Moving Group

Object	$\alpha_{2000.0}$ (h m s)	$\delta_{2000.0}$ (° ′ ″)	*d* (pc)	$\log(L_X/L_{bol})$[a] (dex)	EW(Hα) (Å)	EW(Li) (mÅ)	P_{rot} (days)	NUV–*J* (mag)	FUV–*J* (mag)	References
2M0034+2523	00 34 08.43	+25 23 49.8	48	−3.23 ± 0.10	−0.82	⋯	3.16	10.12 ± 0.07	12.3 ± 0.4	1, 2, 3
HIP 25283	05 24 30.17	−38 58 10.7	18	−3.64 ± 0.04	⋯	12	9.34	⋯	⋯	4, 5, 6
HIP 26369	05 36 55.10	−47 57 48.1	26	−3.36 ± 0.21	−0.9	70	4.54	⋯	⋯	4, 5, 7
HIP 31878	06 39 50.04	−61 28 41.8	22.4	−3.82 ± 0.15	⋯	50	9.06	10.41 ± 0.03	13.1 ± 0.13	4, 6, 7, 8
HIP 86346	17 38 39.65	+61 14 16.1	33	−3.04 ± 0.06	−1.3	40	1.842	9.36 ± 0.04	11.14 ± 0.03	4, 8, 9, 10
2M2039+0620	20 39 54.60	+06 20 11.8	38.5	−3.95 ± 0.12	0.3	⋯	⋯	⋯	⋯	1, 2
HIP 106231	21 31 01.71	+23 20 07.5	24.8	−3.10 ± 0.09	⋯	215	0.423	9.04 ± 0.03	⋯	4, 7, 11
HIP 113597	23 00 27.92	−26 18 43.17	30	−3.68	−0.1	10	8.0	10.47 ± 0.02	12.97 ± 0.13	4 , 11, 12 , 13
2M2236+4751	22 36 24.52	+47 51 42.5	63	<3.1	0.18	<50	11.2	10.9 ± 0.2	⋯	14, 15

Note.
[a] Fractional X-ray luminosities are computed using *ROSAT* count rates following Bowler et al. (2013).
References. (1) McCarthy & White (2012), (2) Lépine et al. (2013), (3) Norton et al. (2007), (4) van Leeuwen (2007), (5) Torres et al. (2006), (6) Messina et al. (2010), (7) Kiraga (2012), (8) Fernández et al. (2008), (9) Gizis et al. (2002), (10) Henry et al. (1995), (11) da Silva et al. (2009), (12) Riaz et al. (2006), (13) Messina et al. (2011), (14) This work; (15) Hartman et al. (2011).

they exhibit a large spread in initial angular momenta, which continues to broaden over time (e.g., Irwin et al. 2011; Mcquillan et al. 2014). Hartman et al. (2011) measure a period of 11.2 days for 2M2236+4751; compared to the Pleaides rotation distribution, which has a comparable age to AB Dor and a well characterized stellar population, this period sits near the maximum envelope of rotation rates for stellar masses of $\approx$0.6 $M_\odot$ (Hartman et al. 2010; Covey et al. 2016; Rebull et al. 2016). K7 members in AB Dor exhibit a similarly broad range of rotation periods from 0.4–9.3 days (Table 3).

Altogether, we find that the kinematics and rotation period of 2M2236+4751 are consistent with the AB Dor moving group. There is some tension between the heliocentric galactic *Y* position compared to accepted members, and similarly the

Table 4
Properties of the 2MASS J22362452+4751425 Ab System

Property	2M2236+4751 A	2M2236+4751 b	References
Astrometry and Kinematics			
$\mu_\alpha \cos\delta$ (mas yr^{-1})	62.6 ± 1.4	…	1
μ_δ (mas yr^{-1})	−30.5 ± 1.9	…	1
$d_{\rm kin}$ (pc)[a]	63 ± 5	…	2
$d_{\rm phot}$ (pc)	74 ± 10	…	2
$RV_{\rm kin}$ (km s^{-1})[a]	−22.8 ± 1.2	…	2
$RV_{\rm ESPaDOnS}$ (km s^{-1})	−22.1 ± 0.5	…	2
$RV_{\rm IGRINS}$ (km s^{-1})	−21.4 ± 0.2	…	2
$\overline{RV}$ (km s^{-1})[b]	−21.5 ± 0.2	…	2
UVW (km s^{-1})[c]	−6.9 ± 1.0, −25.9 ± 0.4, −13.7 ± 1.5		2
XYZ (pc)[c]	−11.6 ± 0.9, 61.1 ± 4.8, −10.0 ± 0.8		2
Photometry			
ΔJ(mag)[d]	9.99 ± 0.11		2
ΔH (mag)[d]	9.16 ± 0.18		2
ΔKs (mag)[d]	8.2 ± 0.04		2
GALEX NUV (mag)	20.9 ± 0.2	…	3
B (mag)	13.73 ± 0.18	…	4
V (mag)	12.51 ± 0.03	…	4
$g'_{\rm APASS}$ (mag)	13.1 ± 0.2	…	4
$r'_{\rm APASS}$ (mag)	11.91 ± 0.03	…	4
$i'_{\rm APASS}$ (mag)	11.32 ± 0.08	…	4
$R2$ (mag)	11.5	…	5
$J_{\rm MKO}$ (mag)	9.975 ± 0.022[e]	19.97 ± 0.11	2, 6
$H_{\rm MKO}$ (mag)	9.388 ± 0.021[e]	18.54 ± 0.18	2, 6
$K_{\rm MKO}$ (mag)	[9.180 ± 0.018][f]	[17.28 ± 0.04][f]	2, 6
K_s (mag)	9.148 ± 0.018	17.35 ± 0.04	2, 6
$W1$ (mag)	9.058 ± 0.023	…	7
$W2$ (mag)	9.094 ± 0.020	…	7
$W3$ (mag)	8.947 ± 0.027	…	7
$W4$ (mag)	8.731 ± 0.356	…	7
$(J-H)_{\rm MKO}$ (mag)	0.59 ± 0.03	1.4 ± 0.2	2, 6
$(H-K)_{\rm MKO}$ (mag)	[0.132 ± 0.001]	[1.26 ± 0.18]	2, 6
$(J-K)_{\rm MKO}$ (mag)	[0.747 ± 0.001]	[2.69 ± 0.12]	2, 6
$H_{\rm MKO} - Ks$ (mag)	0.24 ± 0.03	1.19 ± 0.18	2, 6
$J_{\rm MKO} - Ks$ (mag)	0.827 ± 0.03	2.62 ± 0.12	2, 6
$M_{J_{\rm MKO}}$ (mag)[g]	5.97 ± 0.17	15.97 ± 0.2	2
$M_{H_{\rm MKO}}$ (mag)[g]	5.39 ± 0.17	14.5 ± 0.3	2
M_{K_S} (mag)[g]	5.15 ± 0.17	13.35 ± 0.18	2
$M_{K_{\rm MKO}}$ (mag)[g]	[5.18 ± 0.17]	[13.28 ± 0.18]	2
Physical Properties			
Separation ($''$)	3.70		2
Separation (AU)[g]	230 ± 20		2
Age (Myr)[a]	120 ± 10		8
$\log(L_{\rm bol}/L_\odot)$	−1.17 ± 0.08	−4.57 ± 0.06	2
Mass	0.60 ± 0.05 $M_\odot$	11–14 $M_{\rm Jup}$	2
Spectral Type	[K7 ± 1][h]	late-L pec	2

Notes.
[a] Assumes membership in AB Dor.
[b] Weighted mean of IGRINS and ESPaDOnS radial velocities.
[c] U and X are positive toward the galactic center, V and Y are positive toward the direction of galactic rotation, and W and Z are positive toward the north galactic pole.
[d] Weighted mean of relative photometry from Table 1.
[e] Assumes $J_{\rm MKO} \approx J_{\rm 2MASS}$ and $H_{\rm MKO} \approx H_{\rm 2MASS}$ for 2M2236+4751 A.
[f] Based on synthetic K_S–$K_{\rm MKO}$ color from our SpeX spectrum of the primary (K_S–$K_{\rm MKO}$ = –0.0320 ± 0.0008 mag) and our OSIRIS spectrum of the companion (K_S–$K_{\rm MKO}$ = 0.070 ± 0.004 mag).
[g] Assumes kinematic distance to the host.
[h] Estimated spectral type based on photometry.

References. (1) UCAC4 (Zacharias et al. 2013), (2) This work, (3) Morrissey et al. (2007), (4) APASS (Henden et al. 2016), (5) USNO-B1.0 (Monet et al. 2003), (6) 2MASS (Cutri et al. 2003), (7) *WISE* (Cutri et al. 2012), (8) Torres et al. (2008).

activity level of 2M2236+4751 appears to be lower than AB Dor members of the same spectral type, but neither of these decisively rule out membership. We conclude that 2M2236 +4751 is either an inactive member of AB Dor, presumably in the quiet tail end of the activity distribution, or it is an older kinematic interloper in this group. The unusually red spectrum of the companion may suggest the system is indeed a member of this group, similar to the dusty L dwarf WISE J0047+6803 (Gizis et al. 2012; Gizis et al. 2015). Because of the excellent kinematic agreement with AB Dor, we adopt the cluster age of ≈120 Myr for this work (Luhman et al. 2005; Barenfeld et al. 2013), but note that older ages are also possible if further investigation shows it is not a member.

3.3. Search for Wide Stellar Companions

Wide stellar companions to exoplanet host stars provide a more complete view of the system architecture and offer an independent way to age-date the planet (e.g., Mamajek 2012). We searched for companions to 2M2236+4751 Ab by querying the PPMXL proper motion catalog (Roeser et al. 2010) at separations corresponding to 5000, 10^4, and 10^5 AU. Wu et al. (2011) found that PPMXL proper motions have systematic errors of ≈–2 ± 5 mas yr^{-1} based on a large calibration using stationary quasars. We, therefore, add this systematic uncertainty in quadrature with all objects returned in our search, then compute the difference in proper motions between 2M2236 +4751 and stars within each specified angular radius (Figure 7). Uncertainties are propagated analytically and all stars within 3-σ are considered to be candidate comoving companions.

Real stellar companions should sit on or above the main sequence at the distance to 2M2236+4751, and so we also impose a color–magnitude diagram cut to further vet the sample. V and K_S-band magnitudes are queried from UCAC4; objects falling below the main sequence as determined by Pecaut & Mamajek (2013)[14] in M_V versus V–K_S are excluded from consideration.

Aside from the host star itself, no candidate companions emerged in our 5000 and 10^4 AU searches. Within 10^5 AU, 77 stars have proper motions within $<3\sigma$ of 2M2236+4751. Based on the same analysis for an offset field 2° away, the expectation value for the number of stars having consistent proper motions by chance is 34, and the probability of finding at least one star consistent with 2M2236+4751 is effectively 1.0 from binomial statistics. However, none of these candidates also have V-band magnitudes and fall on or above the main sequence. The probability of at last one star passing all these criteria by chance (absolute V-band magnitude above the main sequence and consistent proper motion) based on our offset field is only 0.28. Altogether, no promising stellar companions emerged in our search.

3.4. Physical Properties of 2M2236+4751 A

No spectral type for 2M2236+4751 A is evident in the literature, but its optical through near-infrared colors suggest ∼K7. For example, its B–V color of 1.2 ± 0.2 mag, V–K_S color of 3.36 ± 0.03 mag, and g'–r' color of 0.59 ± 0.09 mag are all consistent with K7–M0 types (Drilling & Landolt 2000; Tokunaga 2000; Bochanski et al. 2007). This agrees with the estimate of K7 from Lépine & Gaidos (2011) based on V–J

[14] Absolute V-band magnitudes compiled by E. Mamajek can be found at http://www.pas.rochester.edu/∼emamajek/

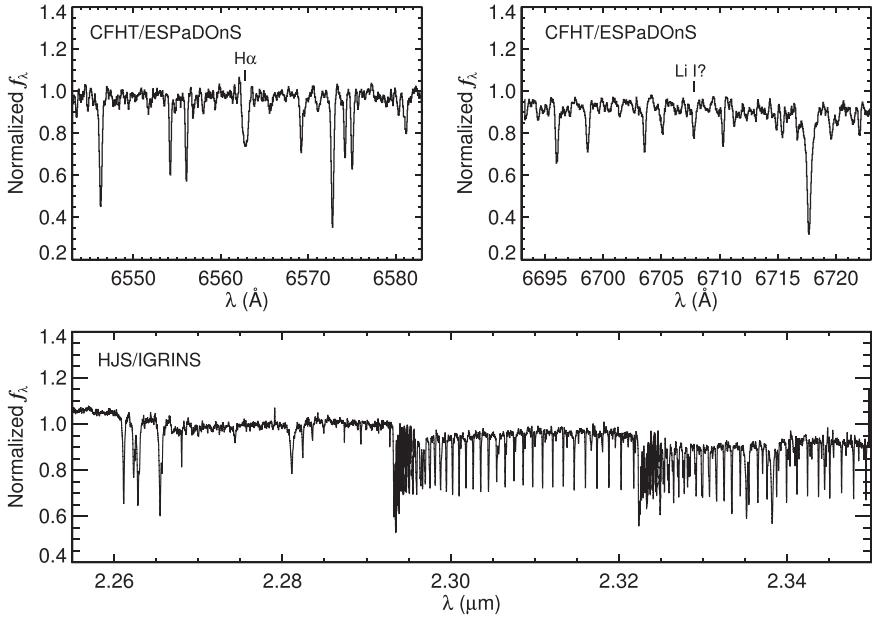

Figure 6. High-resolution optical and near-infrared spectra from CFHT/ESPaDOnS (top panels) and HJS/IGRINS (bottom), respectively. 2M2236+4751 A shows Hα absorption and possible Li I doublet absorption at 6707.8 Å, although this may instead originate from Fe I at 6707.4 Å. The ^{12}CO $\nu = 2$–0 and $\nu = 3$–1 band heads at 2.2935 and 2.3227 μm are visible in our IGRINS data. The ESPaDOnS spectrum has been shifted by +22.1 km s^{-1} to account for its radial velocity.

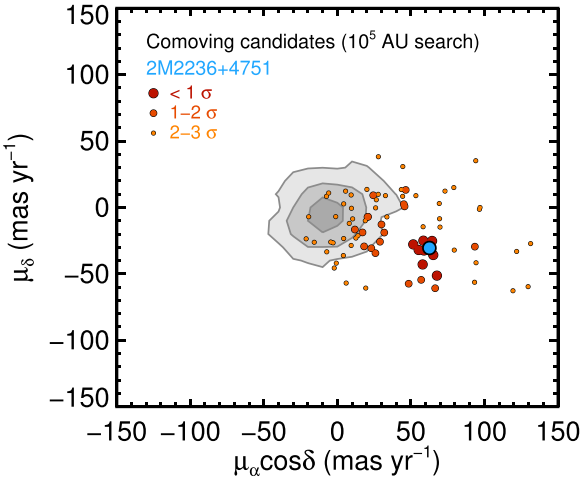

Figure 7. Search for wide stellar companions in the PPMXL proper motion catalog out to 10^5 AU from 2M2236+4751. Gray shaded regions centered at ($\mu_\alpha \cos\delta$, μ_δ) = (0, 0) mas yr^{-1} show contours encapsulating 68%, 90%, and 95% of the field population in the direction of 2M2236+4751. Candidates within 1-, 2-, and 3-σ of 2M2236+4751 are shown as red and orange filled circles. Although 78 stars are consistent within 3-σ, none of those with V-band magnitudes fall on or above the main sequence at the distance of 2M2236+4751.

color. Furthermore, our SpeX spectrum of 2M2236+4751 A shows slight steam absorption at ~1.4 and ~1.9 μm and is most similar to the M0 template from the IRTF Spectral Library (Figure 8; Rayner et al. 2009). Altogether, we estimate a spectral type of [K7 ± 1], where the brackets indicate it is predominantly photometrically based.

We estimate a bolometric luminosity of $\log(L_{\rm bol}/L_\odot) = -1.17 \pm 0.08$ dex for the host star using the H-band bolometric correction from Casagrande et al. (2008) and its kinematic distance. Similarly, we estimate an effective temperature of 4045 ± 35 K from their $T_{\rm eff}$(V–J) relation. The corresponding mass using the Baraffe et al. (2015) evolutionary models and based on the bolometric luminosity and age (120 Myr) is 0.60 ± 0.05 $M_\odot$ (Table 4). This inferred mass is independent of older ages, and so the same value is expected if this system is a kinematic interloper in AB Dor.

3.5. Photospheric and Physical Properties of 2M2236+4751 b

With a J–K_S color of 2.62 ± 0.12 mag and a J–H color of 1.4 ± 0.2 mag, the near-infrared spectral energy distribution of 2M2236+4751 b is among the reddest L dwarfs known. The J–K_S color in particular rivals the most extreme objects in the color–magnitude diagram like 2M1207–3932 b (Chauvin et al. 2004), PSO J318.5–22 (Liu et al. 2013b), HR 8799 b (Marois et al. 2008b), and VHS J1256–1257 b (Gauza et al. 2015), whose unusual spectra are thought to be caused by extremely thick photospheric clouds.

Figure 9 shows our NIRC2 photometry and our K-band OSIRIS spectrum of 2M2236+4751 b. The 1.2–2.2 μm spectral shape and K-band spectrum closely match the near-infrared spectrum of PSO J318.5–22, a 5–8 $M_{\rm Jup}$ L7 VL-G member of β Pic (Liu et al. 2013b; Allers et al. 2016). The 2.3 μm ^{12}CO bandhead and red 2.0–2.2 μm spectral slope are evident in the OSIRIS data. Compared to field L dwarfs and young red L dwarfs in Figure 10, the overall K-band shape of 2M2236+4751 b more closely resembles the latter population of objects with very low and intermediate gravity classifications. Allers & Liu (2013) show that a K-band spectrum alone is not sufficient for precise spectral and gravity classifications of young L dwarfs; lacking broader spectral coverage, we adopt "late-L pec" for 2M2236+4751 b.

A shallow indentation is visible in the pseudo-continuum of our OSIRIS spectrum from ≈2.2–2.3 μm, which is similar to the onset of methane absorption in the latest field L dwarfs. To more quantitatively assess whether this feature is indeed from methane, we compared our spectrum with molecular templates of pure H_2O, CO, and CH_4 following Konopacky et al. (2013) and Barman et al. (2015). The templates were generated by computing a customized thermal emission model using the

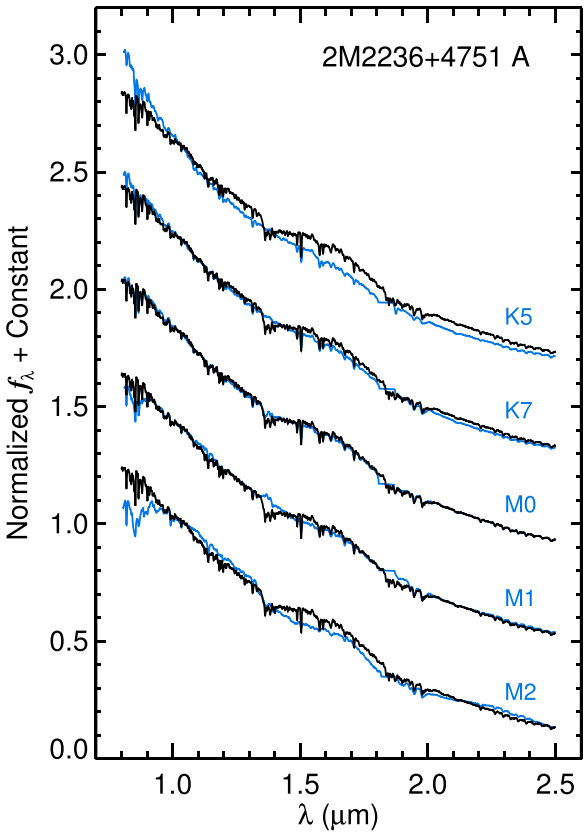

Figure 8. IRTF/SpeX near-infrared spectrum of 2M2236+4751 A (black) compared with K5–M2 dwarf templates from the IRTF Spectral Library (blue; Rayner et al. 2009). 2M2236+4751 A shows slight steam absorption at ∼1.4 and ∼1.9 μm and is most similar to the M0 template. However, the optical colors of the host are slightly bluer than expected for M0, and so we adopt a [K7 ± 1] classification.

SCARLET atmospheric retrieval framework (Benneke 2015). The model self-consistently calculates the thermal structure and equilibrium chemistry at $T_{\rm eff} = 1200$ K for a cloud-free atmosphere with solar elemental composition at a resolving power of $R > 250{,}000$.[15] The molecular templates are then convolved with the instrument profile, flattened by fitting a high-order polynomial, and cross-correlated with the our flattened K-band spectrum.

Results of the cross-correlation are shown in Figure 11 along with the same analysis for M, L, and T dwarfs from the IRTF Spectral Library (Cushing et al. 2005; Rayner et al. 2009). Water shows a significant peak with no cross-correlation lag (velocity shift) in all MLT templates. As expected, the transition from L to T dwarfs is marked by a reduced strength in CO power and an increase in broad methane cross-correlation peak. Although the M dwarfs show substantial power from the CH_4 template, this is a result of the strong 2.2 μm methane absorption feature locking onto the 2.21 μm Na I doublet at high temperatures. For 2M2236+4751 b, we find strong evidence of CO, some evidence of H_2O, and no sign of methane absorption. The slight trough from 2.2–2.3 μm in our OSIRIS spectrum is, therefore, probably not a result of methane absorption.

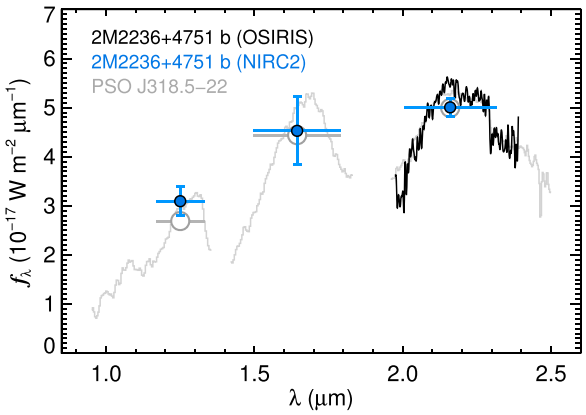

Figure 9. Near-infrared spectral energy distribution of 2M2236+4751 b. Blue points display our NIRC2 photometry of the companion, and our OSIRIS spectrum (smoothed from $R \sim 3800$ to $R \sim 1000$) is shown in black. The near-IR spectrum of PSO J318.5–22 from Liu et al. (2013b) is shown in gray for comparison along with synthetic (scaled) photometry.

We estimate a bolometric luminosity for 2M2236+4751 b using the 0.9–2.4 μm spectrum of PSO J318.5–22 from Liu et al. (2013b)—which bears a close resemblance to 2M2236+4751 b—flux-calibrated to the K_S-band photometry of 2M2236+4751 b together with a [$T_{\rm eff} = 1100$ K; $\log g = 4.5$ dex] BT-Settl atmospheric model from Baraffe et al. (2015) as a bolometric correction at short ($\lambda < 0.9$ μm) and long ($\lambda > 2.4$ μm) wavelengths. Filippazzo et al. (2015) show that the flux redistribution from short to long wavelengths for young L dwarfs pivots between 1.5 and 2.5 μm, and so the atmospheric model parameters for our luminosity calculation are chosen to correspond to the M_H- and M_{KS}-band magnitudes of 2M2236+4751 b predicted by Cond evolutionary models (Baraffe et al. 2003).[16] This effective temperature is consistent with the value from the Filippazzo et al. (2015) young $T_{\rm eff}(M_H)$ relation, which yields 970 ± 150 K for 2M2236+4751 b. Uncertainties in $L_{\rm bol}$ are derived in a Monte Carlo fashion by randomly and repeatedly sampling new distances and absolute flux calibration scale factors from normal distributions based on our kinematic distance estimate (63 ± 5 pc) and apparent K_S magnitude of 2M2236+4751 b (13.35 ± 0.18 mag). We estimate a luminosity of $\log(L_{\rm bol}/L_\odot) = -4.57 \pm 0.06$ dex from the mean and standard deviation of 10^4 trials.

The inferred mass of 2M2236+4751 b is 13.3 ± 0.8 $M_{\rm Jup}$ based on its age, its bolometric luminosity, and the "hybrid" evolutionary models of Saumon & Marley (2008). (The corresponding effective temperature from these models is 1170 ± 40 K.) Using absolute magnitudes instead of bolometric luminosity, we find masses of ≈8, ≈11, and ≈11 $M_{\rm Jup}$ for M_J, M_H, and M_{KS}-band magnitudes based on the Cond evolutionary models of Baraffe et al. (2003). Dusty models from Chabrier et al. (2000) imply an upper limit of <12.5 $M_{\rm Jup}$. Altogether, we adopt a mass range of 11–14 $M_{\rm Jup}$ for 2M2236+4751 b assuming the system is a member of AB Dor. In the unlikely case it is a kinematic interloper, the inferred mass of the companion is 43 ± 5 $M_{\rm Jup}$, 70 ± 2 $M_{\rm Jup}$,

[15] The SCARLET model considers the molecular opacities of H_2O, CH_4, NH_3, HCN, CO, CO_2, and TiO from the high-temperature ExoMol database (Tennyson & Yurchenko 2012); O_2, O_3, OH, C_2H_2, C_2H_4, C_2H_6, H_2O_2, and HO_2 from the HITRAN database (Rothman et al. 2009); and H_2-broadening following the prescription in Burrows & Volobuyev (2003). Collision-induced broadening from H_2/H_2 and H_2/He collisions is computed following Borysow (2002).

[16] Dusty evolutionary models (Chabrier et al. 2000) are truncated at 0.012 $M_\odot$ for an age of 120 Myr, but imply similar upper limits on the physical properties of 2M2236+4751 b: $T_{\rm eff} < 1300$ K, $\log g < 4.2$ dex, and $M < 12.5$ $M_{\rm Jup}$.

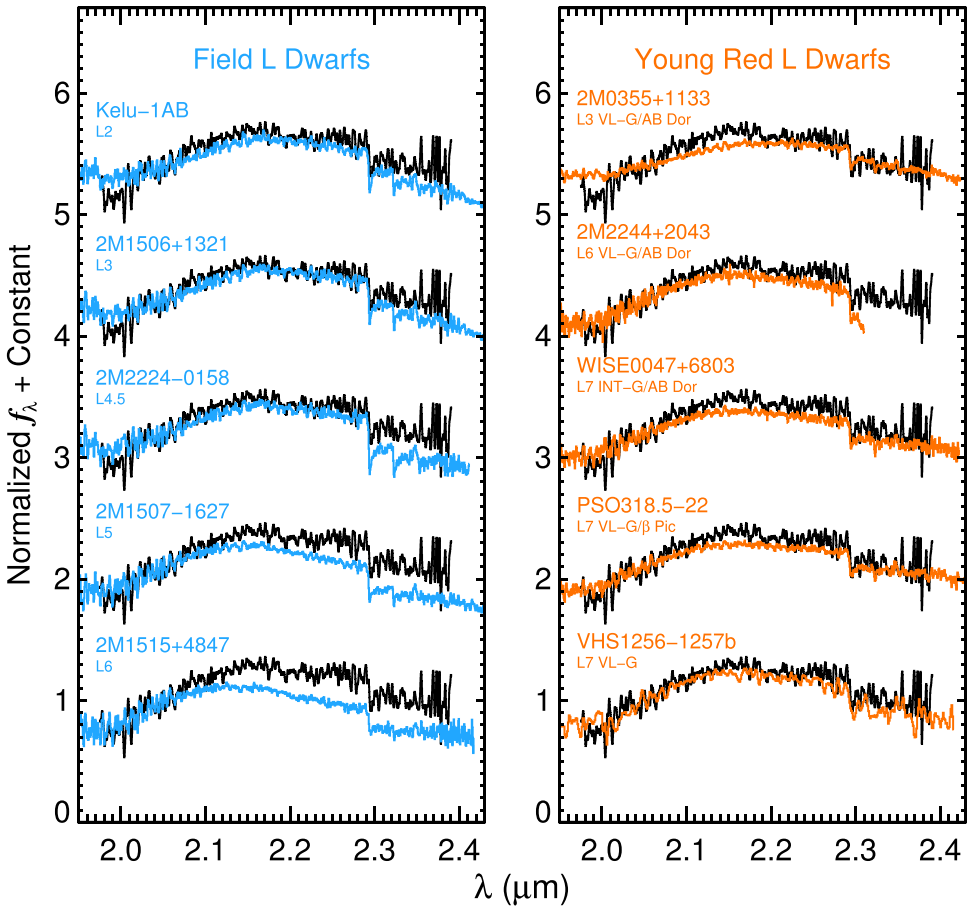

Figure 10. *K*-band spectrum of 2M2236+4751 b compared with field L dwarfs (blue; left panel) and young red L dwarfs (orange; right panel). The overall 2.0–2.1 μm slope and CO strength is most consistent with red late-L dwarfs like PSO J318.5–22 and VHS J1256–1257 b, though broader coverage is needed for a more accurate classification. Comparison spectra are from Cushing et al. (2005) and Rayner et al. (2009) for field L dwarfs and Allers & Liu (2013), McLean et al. (2003), Gizis et al. (2015), Liu et al. (2013b), and Gauza et al. (2015) for red L dwarfs.

and $74 \pm 1\ M_{\rm Jup}$ at ages of 1, 5, and 10 Gyr. The corresponding effective temperatures are 1310 ± 50 K, 1390 ± 40 K, and 1390 ± 40 K for the same ages. Additional photometry—especially at mid-infrared wavelengths—will help to better constrain the luminosity and mass of this remarkable companion.

4. DISCUSSION

Empirical sequences of substellar isochrones in color–magnitude diagrams are important tools to chart the physical and spectral properties of brown dwarfs and giant planets at a given age, map their entire cooling history at a given mass, and jointly test low-temperature atmospheric and evolutionary models. The positions of young (∼10–200 Myr) substellar objects in near-infrared color–magnitude diagrams have progressively come into focus with programs searching for low-mass members of young moving groups (Gagné et al. 2014; Aller et al. 2016) and gas giant planets with high-contrast imaging (Bowler 2016) together with follow-up parallax programs to measure distances (Faherty et al. 2016; Liu et al. 2016). This is particularly true for the young late-M through mid-L dwarf populations, whose numbers and trigonometric distances have swelled in recent years, but the location of young late-L, L/T, and T dwarfs have largely remained elusive owing to the relative dearth of discoveries in this regime and their intrinsic scarcity.

The AB Dor moving group is among the oldest of the nearby ($\lesssim$100 pc) young ($\lesssim$200 Myr) comoving associations in the solar neighborhood (e.g., Zuckerman & Song 2004; Torres et al. 2008). With an age of $\sim 120 \pm 10$ Myr, it straddles younger well characterized moving groups like β Pic and Tuc-Hor at 20–50 Myr and older, more heavily populated clusters at 500–800 Myr like Ursa Majoris, the Hydes, and Coma Ber (Mamajek 2016), thereby serving as an important benchmark for stellar and substellar evolution. The population of confirmed or suspected free-floating brown dwarfs in AB Dor now includes over a dozen objects spanning the entire L dwarf sequence down to ∼T1 (e.g., Best et al. 2015; Aller et al. 2016) as well as the single mid-T dwarf candidate SDSS J1110+0116 (Gagné et al. 2015a). Many brown dwarf and planetary-mass companions have also been identified with masses ranging from roughly 9–40 $M_{\rm Jup}$ (Figure 12): 1RXS J2351+3127 B (L0; Bowler et al. 2012), CD-35 2722 B (L3; Wahhaj et al. 2011), 2M0122–2439 B (L4; Bowler et al. 2013), and GU Psc b (T3.5; Naud et al. 2014). Altogether, this is the largest set of substellar companions for any young moving group.

With a mass of 11–14 $M_{\rm Jup}$, 2M2236+4751 b is the second lowest-mass companion discovered in AB Dor after GU Psc b ($11 \pm 2\ M_{\rm Jup}$; Figure 12). 2M2236+4751 b is also the reddest known member of this group and resides in a prominent position at the "elbow" of its substellar isochrone (Figure 13). It has an even more extreme color than

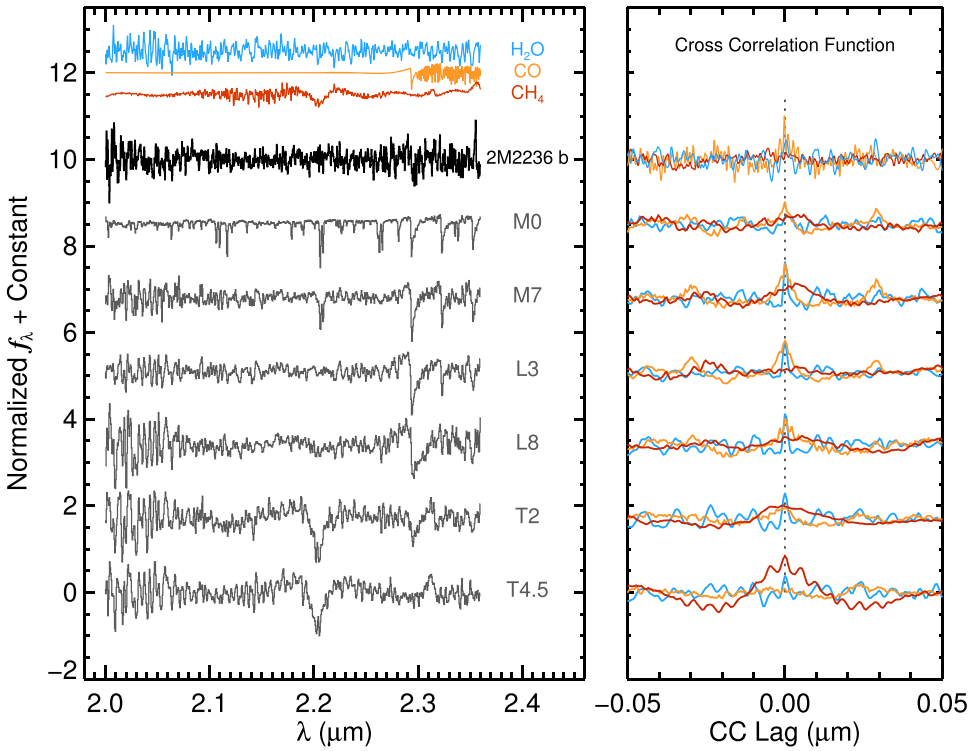

Figure 11. Cross-correlation of pure H_2O, CO, and CH_4 templates with the flattened *K*-band spectrum of 2M2236+4751 b and MLT templates from the IRTF Spectral Library. The cross-correlation function (CCF) power for CO (orange) is strong in M and L dwarfs, then diminishes for T dwarfs as methane (red) becomes the dominant carbon carrier. Water absorption (blue) is evident in all objects, but is noticeably weaker in the mid-T dwarf spectrum. For 2M2236+4751 b, CO is prominent in the CCF, water is weak, and we find no evidence for methane, despite its cool effective temperature of ≈900–1200 K.

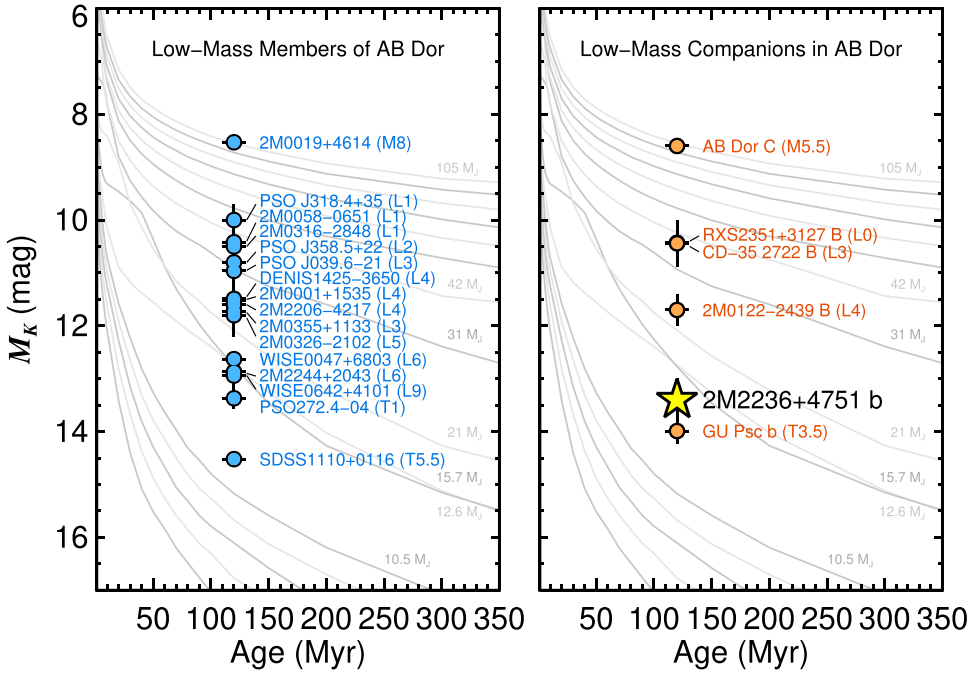

Figure 12. Confirmed and candidate ultracool members of the AB Dor young moving group. In absolute *K*-band magnitude, 2M2236+4751 b (yellow star) is fainter than all isolated brown dwarfs (left) except the T5.5 object SDSS J1110+0116 (Gagné et al. 2015a), and among companions it is the second lowest-mass member after GU Psc b (Naud et al. 2014). BT-Settl evolutionary models are depicted in gray (Baraffe et al. 2015).

two red free-floating brown dwarfs in AB Dor, WISE J0047+6803 ($(J–K)_{MKO} = 2.48 \pm 0.08$ mag) and 2M2244+2043 ($(J–K)_{MKO} = 2.43 \pm 0.04$ mag), demonstrating that the tip of the L dwarf sequence extends to at least $(J–K)_{MKO} = 2.7$ mag even at the relatively old age of this cluster.

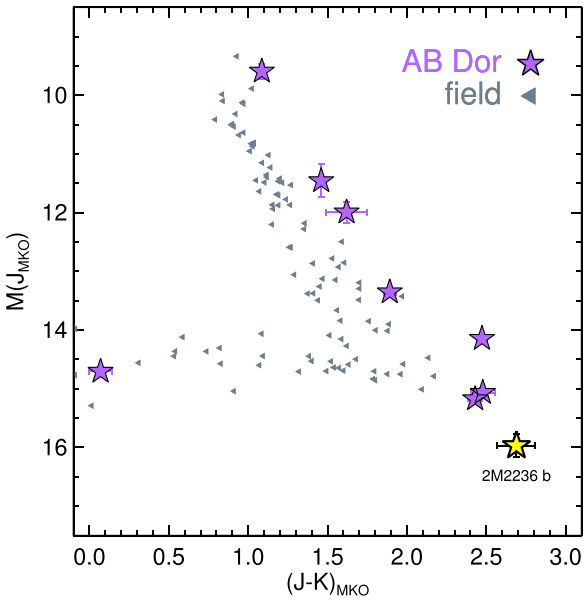

Figure 13. Color–magnitude diagram showing the position of 2M2236+4751 b compared to ultracool members of the AB Dor moving group with parallactic distances and high membership probability as summarized by Liu et al. (2016). We also include PSO J318.4243+35.1277 from Aller et al. (2016), though we do not plot the other two objects in that paper with parallaxes (PSO J039.6352–21.7746 and PSO J358.5527+22.1393) as radial velocity followup by K. Aller (2016, private communication) leads to inconclusive membership results. Normal ultracool field objects are shown as small gray triangles from Dupuy & Liu (2012) for objects with apparent magnitude errors <0.10 mag in J and K and with J-band absolute magnitude errors of <0.10 mag.

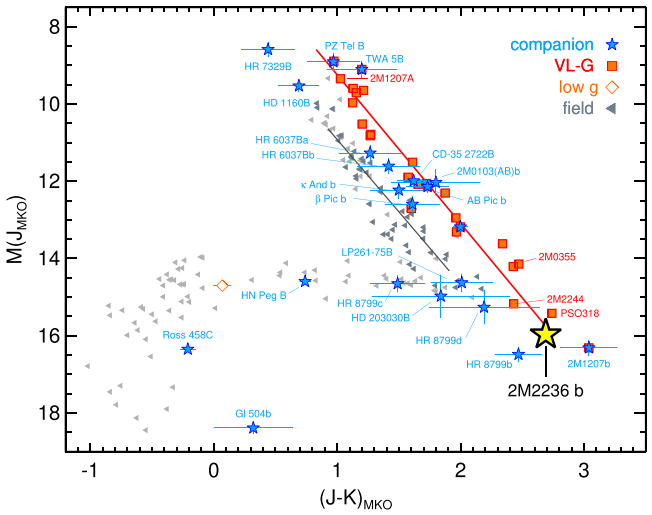

Figure 14. The ultracool $J_{(MKO)}/(J–K)_{(MKO)}$ color–magnitude diagram (adapted from Liu et al. 2016). Triangles denote field brown dwarfs from Dupuy & Liu (2012), filled squares show late-M and L dwarfs with very low-gravity classifications (Liu et al. 2016), and blue stars represent companions with trigonometric distances. 2M2236+4751 b (yellow star) is located at the tip of the faint red L dwarf sequence in a sparsely populated region characterized by extreme cloud properties. Gray and red lines show the linear fit of FLD-G and VL-G brown dwarfs from Liu et al. (2016).

The shape of the AB Dor substellar isochrone has important implications for other clusters with similar ages. The Pleiades is an especially interesting example with a comparable age of about 125 Myr (Stauffer et al. 1998) and possible dynamical relationship with the AB Dor group (Ortega et al. 2007). Although it is one of the best-characterized nearby open clusters with a population of over one thousand stars (e.g., Stauffer et al. 2007), its very low-mass substellar members have been difficult to explore owing to their intrinsic faintness. Nevertheless, several deep near-infrared imaging surveys have identified L dwarfs down to the planetary-mass regime (e.g., Bihain et al. 2006; Lodieu et al. 2007). Zapatero Osorio et al. (2014b) show the Pleiades L dwarf sequence in the $J/J–K$ diagram generally resembles AB Dor, progressively reddening to $J–K$ values of ∼2.5 mag, but then appears to turn over to bluer colors beyond $J \sim 20.3$ mag ($M_J \sim 14.7$ mag) and $K_S \sim 17.8$ mag ($M_{KS} \sim 12.2$ mag; Zapatero Osorio et al. 2014a). However, the absolute magnitudes of 2M2236+4751 b ($M_J = 15.97 \pm 0.2$ mag; $M_{KS} = 13.35 \pm 0.18$ mag) are over one magnitude *fainter* than the location of this apparent turnover. Similarly, the two aforementioned red L dwarfs WISE J0047+6803 and 2M2244+2043 in AB Dor have absolute magnitudes nearly half a magnitude fainter than this possible L/T turnover, suggesting that there is either an age discrepancy between AB Dor and the Pleiades, a dramatic level of photospheric diversity exists among brown dwarfs with similar absolute magnitudes at this age, or that some of the faint blue planetary-mass candidates identified by Zapatero Osorio et al. (2014b) are contaminants.

Compared to other companions, 2M2236+4751 b appears to have even more extreme photospheric properties than all previously known objects, except the ≈5 M_{Jup} object 2M1207–3932 b ($(J–K)_{MKO} = 3.0 \pm 0.2$ mag; Figure 14). However, all isolated objects and companions in this region of the color–magnitude diagram show qualitatively similar atmospheric properties: red colors, faint absolute magnitudes, strong CO absorption, and no signs of methane absorption, despite having effective temperatures below the traditional L/T transition of ≈1200–1400 K for the older field population (e.g., Golimowski et al. 2004). Barman et al. (2011b) and Skemer et al. (2014) find that very thick clouds and rapid vertical mixing are required to reproduce the red colors and lack of methane absorption in 2M1207–3932 b, the most extreme object at the tip of the L dwarf sequence, and these traits are likely to apply to 2M2236+4751 b as well. However, Liu et al. (2016) show that another population of red L dwarfs like 2M2148+4003 (Looper et al. 2008) and WISE J2335+4511 (Thompson et al. 2013), which do not appear to be young, can also reside in this part of the color–magnitude diagram, indicating that surface gravity is not the sole underlying explanation for the shared atmospheric traits of these objects. 2M2236+4751 b reinforces the impression that there do not appear to be any obvious differences between the red, faint objects being discovered as companions and the analogous population of isolated free-floating objects.

With a projected separation of 230 AU, 2M2236+4751 b is the latest example of a growing population of planetary-mass companions on wide orbits of several hundred AU (e.g., Bailey et al. 2014; Kraus et al. 2014; Deacon et al. 2016). The origin of these objects is unclear; planet–planet scattering (Veras et al. 2009), the tail end of disk instability (Kratter et al. 2010), and turbulent fragmentation of molecular clouds (Bate 2009) have all been invoked to explain their origin. Bryan et al. (2016) argue against scattering as the dominant origin of this population due to the lack of additional close-in companions in these systems and the dearth of multiple massive (∼10 M_{Jup}) planets uncovered at small separations in radial velocity surveys. In fact, because of their low numbers and lack of

robust statistics, it is unclear whether these objects make up their own population or are part of a broader distribution of giant planets or low-mass brown dwarfs spanning small separations (tens of AU) out to extremely wide separations (thousands of AU). Unlike most of the wide planetary-mass companions currently known, 2M2236+4751 b is part of a well defined survey (to be discussed in more detail in a future publication) and will help clarify the statistical properties of planetary-mass companions on wide orbits around low-mass stars.

5. SUMMARY AND CONCLUSIONS

We have presented the discovery of a faint red L dwarf companion to the late-K dwarf 2MASS J22362452+4751425. The radial velocity and proper motion of the host star are consistent with the 120 Myr AB Dor young moving group. 2M2236+4751 A is relatively inactive, showing partly filled Hα absorption but no X-ray emission or UV excess, suggesting that it is either in the tail end of the AB Dor activity distribution or it is an older kinematic interloper in that group. The unusually red colors of the companion are similar to (but more extreme than) other mid- to late-L dwarfs in AB Dor, possibly bolstering membership likelihood, but the existence of high-gravity brown dwarfs in this part of the color–magnitude diagram means that this trait is not uniquely a sign of youth and low surface gravity. Assuming the pair is indeed a member of AB Dor, the mass of 2M2236+4751 b is 11–14 $M_{\rm Jup}$ from hot start evolutionary models and resides at a projected separation of $\approx$230 AU at the kinematic distance of $\approx$65 pc to the host star. If the system is an older kinematic interloper, then the implied mass of the companion can be as high as $\sim$74 $M_{\rm Jup}$ at 10 Gyr.

The near-infrared colors of 2M2236+4751 b are among the reddest known of any brown dwarf or giant planet. In near-infrared color–magnitude diagrams, it appears to mark the elbow of the AB Dor substellar isochrone between other faint red L dwarfs like WISE J0047+6803 and 2M2244+2043 and the two T dwarfs GU Psc b and SDSS J1110+0116. This implies that the transition from red L dwarfs to dust-free T dwarfs occurs between a narrow mass range of about 11–13 $M_{\rm Jup}$ at an age of $\approx$120 Myr. The colors of 2M2236+4751 b are redder than HR 8799 b, but slightly bluer than 2M1207–3932 b, demonstrating that even intermediate-age giant planets can possess similarly extreme atmospheric properties beyond 100 Myr.

The 2M2236+4751 Ab system is well suited for a broad range of follow-up studies. The age and mass of 2M2236+4751 b will eventually be clarified with a parallax measurement of the host star from *Gaia* to establish whether the system is a member of AB Dor. Follow-up photometry of the companion at both shorter and longer wavelengths will better constrain its luminosity, spectral type, and atmospheric properties. Both low- and high-resolution near-infrared spectroscopy of 2M2236+4751 b can be used to derive spectral and gravity classifications, independently age-date the system through gravity-dependent absorption line depths, measure its projected rotational velocity, and determine its composition and abundance ratios. Finally, 2M2236+4751 b is also an excellent target for variability studies to measure its rotational period and search for signatures of heterogeneity and patchiness in its unusually thick clouds.

We thank A. Kraus for helpful discussions about the age of the host star and the entire Keck Observatory staff for their exceptional support. I.T. was supported by the Department of Astronomy at the University of Texas at Austin through the Cox Endowment and Board of Visitors Funds, as well as a NASA WIYN PI Data Award administered by the NASA Exoplanet Science Institute as part of NN-EXPLORE through the scientific partnership of NASA, the National Science Foundation, and the National Optical Astronomy Observatory. This paper includes data taken at The McDonald Observatory of The University of Texas at Austin. It is also based on observations obtained with ESPaDOnS, located at the Canada–France–Hawaii Telescope (CFHT). CFHT is operated by the National Research Council of Canada, the Institut National des Sciences de l'Univers of the Centre National de la Recherche Scientique of France, and the University of Hawai'i. ESPaDOnS is a collaborative project funded by France (CNRS, MENESR, OMP, LATT), Canada (NSERC), CFHT and ESA. We utilized data products from 2MASS, which is a joint project of the University of Massachusetts and the Infrared Processing and Analysis Center/California Institute of Technology, funded by NASA and the National Science Foundation. NASA's Astrophysics Data System Bibliographic Services together with the VizieR catalogue access tool and SIMBAD database operated at CDS, Strasbourg, France, were invaluable resources for this work. This work used the Immersion Grating Infrared Spectrometer (IGRINS) that was developed under a collaboration between the University of Texas at Austin and the Korea Astronomy and Space Science Institute (KASI) with the financial support of the US National Science Foundation under grant AST-1229522, to the University of Texas at Austin, and of the Korean GMT Project of KASI. This publication makes use of data products from the *Wide-field Infrared Survey Explorer*, which is a joint project of the University of California, Los Angeles, and the Jet Propulsion Laboratory/California Institute of Technology, funded by NASA. Finally, mahalo nui loa to the kama'āina of Hawai'i for their support of Keck and the Maunakea observatories. We are grateful to have been able to conduct observations from this mountain.

Facilities: Keck:II (NIRC2), Keck:I (OSIRIS), Smith (IGRINS), IRTF (SpeX), CFHT (ESPaDOnS).

REFERENCES

Aller, K. M., Liu, M. C., Magnier, E. A., et al. 2016, ApJ, 821, 1
Allers, K. N., Gallimore, J. F., Liu, M. C., & Dupuy, T. J. 2016, ApJ, 819, 1
Allers, K. N., & Liu, M. C. 2013, ApJ, 772, 79
Bailey, V., Meshkat, T., Reiter, M., et al. 2014, ApJL, 780, L4
Baraffe, I., Chabrier, G., Barman, T. S., Allard, F., & Hauschildt, P. H. 2003, A&A, 402, 701
Baraffe, I., Homeier, D., Allard, F., & Chabrier, G. 2015, A&A, 577, A42
Barenfeld, S. A., Bubar, E. J., Mamajek, E. E., & Young, P. A. 2013, ApJ, 766, 6
Barman, T. S., Konopacky, Q. M., Macintosh, B., & Marois, C. 2015, ApJ, 804, 1
Barman, T. S., Macintosh, B., Konopacky, Q. M., & Marois, C. 2011a, ApJ, 733, 65
Barman, T. S., Macintosh, B., Konopacky, Q. M., & Marois, C. 2011b, ApJL, 735, L39
Bate, M. R. 2009, MNRAS, 392, 590
Benneke, B. 2015, arXiv:1504.07655
Best, W. M. J., Liu, M. C., Magnier, E. A., et al. 2015, ApJ, 814, 118
Bihain, G., Rebolo, R., Béjar, V. J. S., et al. 2006, A&A, 458, 805
Bochanski, J. J., West, A. A., Hawley, S. L., & Covey, K. R. 2007, AJ, 133, 531
Bonnefoy, M., Zurlo, A., Baudino, J. L., et al. 2016, A&A, 587, A58
Borysow, A. 2002, A&A, 390, 779

Bowler, B. P. 2016, PASP, 128, 102001
Bowler, B. P., Liu, M. C., Dupuy, T. J., & Cushing, M. C. 2010, ApJ, 723, 850
Bowler, B. P., Liu, M. C., Shkolnik, E. L., et al. 2012, ApJ, 753, 142
Bowler, B. P., Liu, M. C., Shkolnik, E. L., & Dupuy, T. J. 2013, ApJ, 774, 55
Bowler, B. P., Liu, M. C., Shkolnik, E. L., & Tamura, M. 2015, ApJS, 216, 7
Bryan, M. L., Bowler, B. P., Knutson, H. A., et al. 2016, arXiv:1606.06744v1
Burrows, A., & Volobuyev, M. 2003, ApJ, 583, 985
Casagrande, L., Flynn, C., & Bessell, M. 2008, MNRAS, 389, 585
Chabrier, G., Baraffe, I., Allard, F., & Hauschildt, P. 2000, ApJ, 542, 464
Chauvin, G., Lagrange, A.-M., Dumas, C., et al. 2004, A&A, 425, L29
Covey, K. R., Agüeros, M. A., Law, N. M., et al. 2016, ApJ, 822, 81
Cruz, K. L., Kirkpatrick, J. D., & Burgasser, A. J. 2009, AJ, 137, 3345
Cushing, M. C., Rayner, J. T., & Vacca, W. D. 2005, ApJ, 623, 1115
Cushing, M. C., Vacca, W. D., & Rayner, J. T. 2004, PASP, 116, 362
Cutri, R. M., Skrutskie, M. F., Van Dyk, S., et al. 2003, The 2MASS All-Sky Catalog of Point Sources, University of Massachusetts and Infrared Processing and Analysis Center; IPAC/California Institute of Technology
Cutri, R. M., et al. 2012, yCat, 2311, 0
Dahn, C. C., Harris, H. C., Vrba, F. J., et al. 2002, AJ, 124, 1170
da Silva, L., Torres, C. A. O., De La Reza, R., et al. 2009, A&A, 508, 833
Deacon, N. R., Schlieder, J. E., & Murphy, S. J. 2016, MNRAS, 457, 3191
Donati, J.-F., Catala, C., Landstreet, J. D., & Petit, P. 2006, in ASP Conf. Ser. 358, Solar Polarization 4, ed. R. Casini & B. W. Lites (San Francisco, CA: ASP), 362
Donati, J. F., Semel, M., Carter, B. D., Rees, D. E., & Collier-Cameron, A. 1997, MNRAS, 291, 658
Drilling, J. S., & Landolt, A. U. 2000, in Allen's Astrophysical Quantities, ed. A. N. Cox (4th ed.; Melville, NY: AIP, Springer), 381
Dupuy, T. J., & Liu, M. C. 2012, ApJS, 201, 19
Faherty, J. K., Riedel, A. R., Cruz, K. L., et al. 2016, ApJS, 225, 1
Fernández, D., Figueras, F., & Torra, J. 2008, A&A, 480, 735
Filippazzo, J. C., Rice, E. L., Faherty, J., et al. 2015, ApJ, 810, 1
Findeisen, K., Hillenbrand, L., & Soderblom, D. 2011, AJ, 142, 23
Gagné, J., Burgasser, A. J., Faherty, J. K., et al. 2015a, ApJL, 808, 1
Gagné, J., LaFreniere, D., Doyon, R., Malo, L., & Artigau, E. 2014, ApJ, 783, 121
Gagné, J., LaFreniere, D., Doyon, R., Malo, L., & Artigau, E. 2015b, ApJ, 798, 73
Gaidos, E., Mann, A. W., Lépine, S., et al. 2014, MNRAS, 443, 2561
Gauza, B., Bejar, V. J. S., Pérez-Garrido, A., et al. 2015, ApJ, 804, 96
Geißler, K., Metchev, S., Kirkpatrick, J. D., Berriman, G. B., & Looper, D. 2011, ApJ, 732, 56
Gizis, J. E., Allers, K. N., Liu, M. C., et al. 2015, ApJ, 799, 203
Gizis, J. E., Faherty, J. K., Liu, M. C., et al. 2012, AJ, 144, 94
Gizis, J. E., Reid, I. N., & Hawley, S. L. 2002, AJ, 123, 3356
Golimowski, D. A., Leggett, S. K., Marley, M. S., et al. 2004, AJ, 127, 3516
Hartman, J. D., Bakos, G. Ã., Kovács, G., & Noyes, R. W. 2010, MNRAS, 408, 475
Hartman, J. D., Bakos, G. Á., Noyes, R. W., et al. 2011, AJ, 141, 166
Henden, A. A., Templeton, M., & Terrell, D. 2016, yCat, 2336, 0
Henry, G. W., Fekel, F. C., & Hall, D. S. 1995, AJ, 110, 2926
Hinkley, S., Bowler, B. P., Vigan, A., et al. 2015, ApJL, 805, 1
Irwin, J., Berta, Z. K., Burke, C. J., et al. 2011, ApJ, 727, 56
Johnson, D. R. H., & Soderblom, D. R. 1987, AJ, 93, 864
Kellogg, K., Metchev, S., Gagné, J., & Faherty, J. 2016, ApJL, 821, 1
Kiraga, M. 2012, AcA, 62, 67
Kirkpatrick, J. D., Barman, T. S., Burgasser, A. J., et al. 2006, ApJ, 639, 1120
Kirkpatrick, J. D., Cruz, K. L., Barman, T. S., et al. 2008, ApJ, 689, 1295
Konopacky, Q. M., Barman, T. S., Macintosh, B. A., & Marois, C. 2013, Sci, 339, 1398
Kratter, K. M., Murray-Clay, R. A., & Youdin, A. N. 2010, ApJ, 710, 1375
Kraus, A. L., Ireland, M. J., Cieza, L. A., et al. 2014, ApJ, 781, 20
Larkin, J., Barczys, M., Krabbe, A., et al. 2006, Proc. SPIE, 6269, 42
Lee, J.-J., & Gullikson, K. 2016, plp: v2.1 alpha 3
Lépine, S., & Gaidos, E. 2011, AJ, 142, 138
Lépine, S., Hilton, E. J., Mann, A. W., et al. 2013, AJ, 145, 102
Liu, M. C., Dupuy, T. J., & Allers, K. N. 2013a, AN, 334, 85
Liu, M. C., Dupuy, T. J., & Allers, K. N. 2016, APJ, in press
Liu, M. C., Magnier, E. A., Deacon, N. R., et al. 2013b, ApJL, 777, L20
Lodieu, N., Dobbie, P. D., Deacon, N. R., et al. 2007, MNRAS, 380, 712
Looper, D. L., Kirkpatrick, J. D., Cutri, R. M., et al. 2008, ApJ, 686, 528
Luhman, K. L., Stauffer, J. R., & Mamajek, E. E. 2005, ApJL, 628, L69
Mace, G., Kim, H., Jaffe, D. T., et al. 2016, Proc. SPIE, 9908, 99080C
Mace, G. N., Kirkpatrick, J. D., Cushing, M. C., et al. 2013, ApJS, 205, 6
Malo, L., Artigau, E., Doyon, R., et al. 2014, ApJ, 788, 81
Malo, L., Doyon, R., Lafrenière, D., et al. 2013, ApJ, 762, 88
Mamajek, E. E. 2012, ApJL, 754, L20
Mamajek, E. E. 2016, in IAU Symp. 314, Young Stars & Planets Near the Sun (Cambridge: Cambridge Univ. Press), 21
Marocco, F., Day-Jones, A. C., Lucas, P. W., et al. 2014, MNRAS, 439, 372
Marois, C., Lafrenière, D., Macintosh, B., & Doyon, R. 2008a, ApJ, 673, 647
Marois, C., Macintosh, B., Barman, T., et al. 2008b, Sci, 322, 1348
Martin, D. C., Fanson, J., Schiminovich, D., et al. 2005, ApJL, 619, L1
McCarthy, K., & White, R. J. 2012, AJ, 143, 134
McLean, I. S., McGovern, M. R., Burgasser, A. J., et al. 2003, ApJ, 596, 561
Mcquillan, A., Mazeh, T., & Aigrain, S. 2014, ApJS, 211, 24
Messina, S., Desidera, S., Lanzafame, A. C., Turatto, M., & Guinan, E. F. 2011, A&A, 532, A10
Messina, S., Desidera, S., Turatto, M., Lanzafame, A. C., & Guinan, E. F. 2010, A&A, 520, A15
Mieda, E., Wright, S. A., Larkin, J. E., et al. 2014, PASP, 126, 250
Mohanty, S., Jayawardhana, R., Huélamo, N., & Mamajek, E. 2007, ApJ, 657, 1064
Monet, D. G., Levine, S. E., Canzian, B., et al. 2003, AJ, 125, 984
Morrissey, P., Conrow, T., Barlow, T. A., et al. 2007, ApJS, 173, 682
Naud, M.-E., Artigau, E., Malo, L., et al. 2014, ApJ, 787, 5
Norton, A. J., Wheatley, P. J., West, R. G., et al. 2007, A&A, 467, 785
Ortega, V. G., Jilinski, E., De La Reza, R., & Bazzanella, B. 2007, MNRAS, 377, 441
Park, C., Jaffe, D. T., Yuk, I.-S., et al. 2014, Proc. SPIE, 9147, 91471D
Patience, J., King, R. R., De Rosa, R. J., & Marois, C. 2010, A&A, 517, A76
Pecaut, M. J., & Mamajek, E. E. 2013, ApJS, 208, 9
Preibisch, T., & Feigelson, E. D. 2005, ApJS, 160, 390
Rayner, J. T., Cushing, M. C., & Vacca, W. D. 2009, ApJS, 185, 289
Rayner, J. T., Toomey, D. W., Onaka, P. M., et al. 2003, PASP, 115, 362
Rebull, L. M., Stauffer, J. R., Bouvier, J., et al. 2016, arXiv:1606.00052v1
Reid, I. N., Cruz, K. L., Kirkpatrick, J. D., et al. 2008, AJ, 136, 1290
Riaz, B., Gizis, J. E., & Harvin, J. 2006, AJ, 132, 866
Roeser, S., Demleitner, M., & Schilbach, E. 2010, AJ, 139, 2440
Rothman, L. S., Gordon, I. E., Barbe, A., et al. 2009, JQSRT, 110, 533
Saumon, D., & Marley, M. S. 2008, ApJ, 689, 1327
Schlieder, J. E., Lépine, S., & Simon, M. 2012, AJ, 143, 80
Schneider, A. C., Cushing, M. C., Kirkpatrick, J. D., et al. 2014, AJ, 147, 34
Schneider, A. C., Windsor, J., Cushing, M. C., Kirkpatrick, J. D., & Wright, E. L. 2016, ApJL, 822, 1
Service, M., Lu, J. R., Campbell, R., et al. 2016, PASP, 128, 1
Shkolnik, E. L., & Barman, T. S. 2014, AJ, 148, 64
Shkolnik, E. L., Liu, M. C., Reid, I. N., Dupuy, T., & Weinberger, A. J. 2011, ApJ, 727, 6
Skemer, A. J., Marley, M. S., Hinz, P. M., et al. 2014, ApJ, 792, 17
Skrutskie, M. F., Cutri, R. M., Stiening, R., et al. 2006, AJ, 131, 1163
Stauffer, J. R., Hartmann, L. W., Fazio, G. G., et al. 2007, ApJS, 172, 663
Stauffer, J. R., Schultz, G., & Kirkpatrick, J. D. 1998, ApJL, 499, L199
Tennyson, J., & Yurchenko, S. N. 2012, MNRAS, 425, 21
Thompson, M. A., Kirkpatrick, J. D., Mace, G. N., et al. 2013, PASP, 125, 809
Tokunaga, A. T. 2000, in Allen's Astrophysical Quantities, ed. A. N. Cox (4th ed.; New York: AIP, Springer), 143
Torres, C. A. O., Quast, G. R., da Silva, L., et al. 2006, A&A, 460, 695
Torres, C. A. O., Quast, G. R., Melo, C. H. F., & Sterzik, M. F. 2008, in Young Nearby Loose Associations, ed. B. Reipurth (San Francisco, CA: ASP), 757
Vacca, W. D., Cushing, M. C., & Rayner, J. T. 2003, PASP, 115, 389
van Leeuwen, F. 2007, A&A, 474, 653
Veras, D., Crepp, J. R., & Ford, E. B. 2009, ApJ, 696, 1600
Voges, W., Aschenbach, B., Boller, T., et al. 1999, A&A, 349, 389
Wahhaj, Z., Liu, M. C., Biller, B. A., et al. 2011, ApJ, 729, 139
Wizinowich, P. 2013, PASP, 125, 798
Wu, Z.-Y., Ma, J., & Zhou, X. 2011, PASP, 123, 1313
Yelda, S., Lu, J. R., Ghez, A. M., et al. 2010, ApJ, 725, 331
Zacharias, N., Finch, C. T., Girard, T. M., et al. 2013, AJ, 145, 44
Zahnle, K. J., & Marley, M. S. 2014, ApJ, 797, 41
Zapatero Osorio, M. R., Bejar, V. J. S., Martín, E. L., et al. 2014a, A&A, 572, A67
Zapatero Osorio, M. R., Gálvez-Ortiz, M. C., Bihain, G., et al. 2014b, A&A, 568, A77
Zuckerman, B., & Song, I. 2004, ARA&A, 42, 685